Eur. Phys. J. Spec. Top.
https://doi.org/10.1140/epjs/s11734-023-01070-6

THE EUROPEAN PHYSICAL JOURNAL SPECIAL TOPICS

Regular Article

Triangular tessellations of one-loop scattering amplitudes in ϕ^3 theory

Abhijit B. Das[a]

Centre for High Energy Physics, Indian Institute of Science, Bangalore, Karnataka 560012, India

Received 12 October 2023 / Accepted 7 December 2023

Abstract Inspired by the recent work of Nima Arkani Hamed and collaborators who introduced the notion of positive geometry to account for the structure of tree-level scattering amplitudes in bi-adjoint ϕ^3 theory, which led to one-loop descriptions of the integrands. Here, we consider the one-loop integrals themselves in ϕ^3 theory. In order to achieve this end, the geometrical construction offered by Schnetz for Feynman diagrams is hereby extended, and the results are presented. The extension relies on masking the loop momentum variable with a constant and proceeding with the calculations. The results appear as a construction given in a diagrammatic manner. The significance of the resulting triangular diagrams is that they have a common side amongst themselves for the corresponding Feynman diagrams they pertain to. Further extensions to this mathematical construction can lead to additional insights into higher loops. A mathematica code has been provided in order to generate the final results given the initial parameters of the theory.

1 Introduction

Elementary particle physics has been relying on the properties of Feynman diagrams for over half a century now for precision computations in QED and the Standard Model. They are the fundamental building blocks for our understanding of interactions. Feynman diagrams are often used to compute scattering amplitudes in addition to many other observables. There are several mathematical explorations on various aspects of this, in addition to practical computations. One such important direction has been pursued by Nima Arkani Hamed and collaborators. They have studied the properties of integrands in the framework of positive geometry. On the other hand, there is an interpretation of one-loop integrals themselves with n legs by Schnetz in context of hyperbolic geometry. In this work, we have made the first attempt to combine the two approaches. To this extent, this is an investigation at the forefront of elementary particle physics.

Scattering amplitudes are known to satisfy general properties based on analyticity, unitarity, and crossing symmetry, and there are significant constraints on their behavior in the physical world. On the other hand, Feynman diagrams also suffer from difficulties of many kinds, including the fact that they are often divergent, requiring them to be regularized and the theory to be renormalized. This is now a sophisticated field in itself. Life becomes more complicated as the number of loops increases, as well as the number of mass scales also increases. Furthermore, Feynman integrals have also opened the gates to research in the properties of, e.g., hypergeometric functions, and also have enriched subjects as diverse as algebraic geometry, and their analysis requires knowledge of functional analysis and properties of functions of mathematical physics. Other approaches to their evaluation analytically in certain limits include, e.g., the Method of Regions, Sector Decomposition and obtaining so-called Master Integrals and their epsilon expansion have been developed in differential equations, dispersions relations, etc. In this regard, it must be mentioned that polytopes appear in several contexts in the analysis of Feynman integrals [1–4] and for conformal integrals [5–8]. While finishing our previous works [9, 10], the prime motivation for this work originated from a paper of Abreu [11] where he considers different kinds of polytopes in his cut analysis.

Scattering amplitudes also have had a new life in the recent past due to the extensive work done on them. Scattering amplitudes in perturbative Quantum Field Theory are obtained by summing up the contributing Feynman

[a] e-mails: abhijit@iisc.ac.in; abhijitdas123654@gmail.com (corresponding author)

Published online: 24 January 2024

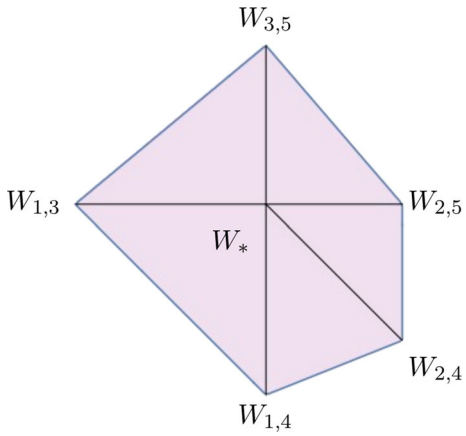

Fig. 1 A particular triangulation of the dual associahedron. Here, W_{ij} are the dual vectors defined in [15]

diagrams at all orders. Being directly observable, they are entities of prime importance in studying elementary particles in experiments in Large Hadron collider and other particle colliders. An excellent review of recent exciting developments made in the subject is done in Elvang and Huang [12] and Henn and Plefka [13].

However, there are also other rich approaches to their study in terms of the amplituhedron [14], associahedron [15]. A nice review of these is given in [16, 17]

In this regard, recently, Nima Arkani Hamed and his co-workers have advocated the study of scattering amplitudes at tree-level within the framework of positive geometries. This has led to a very nice geometric picture encapsulated in Fig. (16) of their paper [15]. This is called as the associahedron polytope. One interesting fact about the associahedron is that in one of the triangulations of the dual associahedron containing a spurious pole, Feynman diagrams emerge as polytopes with common sides and as parts of the bigger associahedron polytope, see Fig. 1. Here, in this picture, the volume of each triangle gives the value of a Feynman diagram contributing to the whole scattering amplitude. The work is at tree-level and has been successfully extended to the integrands at the loop level, [18–20] for biadjoint and ordinary ϕ^3 theory. This has motivated us to look for similar common sides for Feynman diagrams in the loop cases at the integral level. And interestingly, we find similar resemblance for the Feynman diagrams and scattering amplitudes at the integral level discussed in detail in the next two sections. Also, the extension of these to more general theories has been made in [21, 22]

Some years ago, Schnetz [23] studied the geometry of one-loop Feynman integrals in ϕ^3 theory, in which he introduced the mathematical framework, including hyperbolic geometry. This is based on the earlier work of Davydychev and Delbourgo, who construct the basic polytopes [24].

From the above, it may be seen that the issue of one-loop integrals appearing in scattering amplitudes has not been highlighted much (to be contrasted with the one-loop and higher loop integrands in SUSY and other theories). In this direction, some recent work has been done in [25]. The aim of this work is to compute such one-loop integrals in a unified framework. And also, subsequently, the prime motivation is to find a geometry for the S-matrix as a whole, uniting all the loop orders, which is possible if we consider the geometry at the integral level.

In order to achieve this end, we construct formalism, which unifies the loop propagators and the internal propagators. What arises is a generalization of Schnetz that is suitable for representing the scattering amplitude that can be captured in a diagrammatic form. In the work of Schnetz, he considers only primitive one-loop integrals. In contrast, we are led to consider all the one-loop diagrams appearing in a scattering amplitude in the theory for the $N = 3$ case at $n = 3$ dimensions. It is analogous to the set of diagrams appearing in the biadjoint ϕ^3 theory of [15], where only the tree-level amplitudes are considered. The extension to $N = 4$ at $n = 4$ dimensions can be done following similar steps but the exact mathematical framework needs to be more mathematically rigorous and hence is a subject of ongoing investigation as mentioned in the text. Subsequently, the whole information about the scattering amplitude will be inscribed in a 3D picture in contrast to the 2D picture inscription according to the formalism presented in this paper.

The fundamental difference between our case and the positive geometry case is that here we are working at the level of integrals directly. Also, we are restricting ourselves to the $N = 3$ case, where the positive geometry yields a straight line as a special case of the associahedron polytope. It will be interesting to mention that an advancement for finding geometries in the non-perturbative sector has been done in [26].

The scheme of this paper is as follows: In Sect. 2, we start with a short review of Schnetz's work and then proceed to construct our mathematical formalism, which brings together the loop and internal propagators in a single framework. In Sect. 3, we evaluate the general quadric surface equation originating from this framework

for the case of triangle, bubble, and tadpole diagrams. In Sect. 4, we evaluate each diagram and try to give it a geometric representation. In Sect. 5, we try to stack up the contributions coming from all the Feynman integrals in order to provide a diagrammatic representation of the scattering amplitude. Sect. 6 contains the discussions and conclusions.

In the Appendix, we explain the equations which are the central figures in the mathematical formalism of this paper. A stand-alone mathematica code is provided, which explicitly codes the algorithm.

In Sect. 2, until Eq. (19) is a recap of Schnetz. He uses a linear transformation in which the fact that the integration area is a surface integral becomes evident, and the polytope which can be obtained from them becomes obvious. The final result is completely expressed in terms of geometrical quantities in hyperbolic space and the corresponding Euclidean space. Our work extends this work to include other types of one-loop diagrams contributing to the scattering amplitude.

The formalism so far is not enough to address the issue of the entire set of diagrams appearing in the one-loop scattering amplitude and the resulting integrals. Note here that the integrands are considered in [18–20] where the result appears as polytopes (cluster polytopes and halohedron). In contrast, when we complete our construction, the results will also appear as polytopes (triangles) of a different type and with common sides amongst them which is the main result of this paper.

In Sect. 3, we apply the actual values of the masking constants $a_i \to 0, 1$, to get the results of the corresponding one-loop integrals. Here, we discover some new and very interesting facts about the type of hyperbolic geometry obeyed by these integrals. The triangle Feynman diagram for the $N = 3$ case consists of all the three involved masking constants a_i having a value equal to 1; for the bubble, any two are equal to 1, and the third one is zero, and for the tadpole, any one masking constant a_i is equal to one and the rest are equal to zero. From this, we obtain a very interesting fact that the triangle Feynman diagram represents the hyperboloid of two sheets, the bubble represents a rotated hyperboloid of two sheets but with one flat axis, and the tadpole represents a rotated hyperboloid of two sheets with both flat axis.

In Sect. 5, we display the final results. These are displayed by appropriately stacking up the polytopes that we have obtained. This is the analog of the tree-level bi-adjoint stacking of the polytopes given by Nima Arkani Hamed. Though not so mathematically rigorous, the fact that the scattering amplitudes have a geometry of their own in this theory is a significant advance over the simple one-loop formula given by Schnetz.

Future work could be directed at generalizing this picture to higher loops which could help the computation of scattering amplitudes to higher precision and give a completely new and more straightforward method to evaluate scattering amplitudes involving unique and fascinating geometry. Such a unified framework is in philosophy analogous to that of Nima Arkani Hamed for bi-adjoint theories, where the tree-level did not require any loop analysis and where the one-loop has been given only for integrands. In this tree-level context, it has been named the associahedron, whereas at the one-loop level, the integrand polytope construction is called cluster polytopes. Our work is a generalization in a different direction up to the first order in the series expansion.

Appendices include the table showing the correspondence of the individual mapped Feynman diagrams with their generating variables, the derivation of certain key equations, and results.

2 Mathematical construction

2.1 Review

This is a review of the work done in [23]. The most important point about this work is that it extends the geometric formulation of Feynman integrals at the one-loop level using a linear transformation because of which the hyperbolic polytope structure with well-defined boundaries becomes more evident. The one-loop Feynman diagram here is given by

$$A(p_1, m_1, \ldots, p_N, m_N) = \int_{\mathbb{R}^n} \mathrm{d}^n p \frac{1}{Q_1 \cdots Q_N}, \tag{1}$$

with

$$Q_i = (p - p_i)^2 + m_i^2, \quad i = 1, \ldots, N, \tag{2}$$

where p is the loop momentum. The incoming external momenta are

$$p_{i,\,i+1} = p_{i+1} - p_i, \tag{3}$$

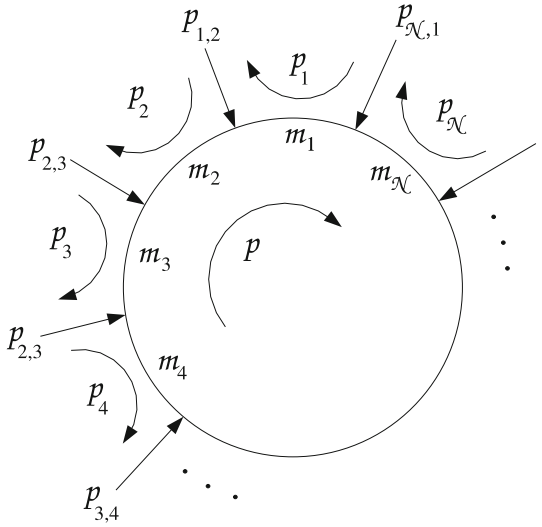

Fig. 2 Feynman diagram of the one-loop amplitude

where $p_{N+1} = p_1$ and $p_{N,\,N+1} = p_{N,\,1}$. Note that these incoming external momenta p_{ij} have fixed magnitude and direction but the internal momenta inside the loop p_i do not have well defined magnitude and direction, only the consecutive difference between them which equals the external momenta are well defined in terms of magnitude and direction. We have used this fact extensively in the construction of our mathematical formalism in the next subsection.

Using α parametrization, we can write the integrand as

$$\frac{1}{Q_1 \cdots Q_N} = (N-1)! \int_0^\infty \mathrm{d}\alpha_2 \cdots \int_0^\infty \mathrm{d}\alpha_N \frac{1}{(Q_1 + \alpha_2 Q_2 + \ldots + \alpha_N Q_N)^N}. \tag{4}$$

Since the integration spans the whole real space, shifting $p \mapsto p + (\sum \alpha_i p_i)/(\sum \alpha_i)$, which is a constant shift, does not alter the value of the integral and we get

$$\int \mathrm{d}^n p \frac{1}{Q_1 \cdots Q_N} = \int_\Delta \Omega \frac{2\pi^{\frac{n}{2}}}{\Gamma(\frac{n}{2})} \int_0^\infty \frac{\mathrm{d}p\, p^{n-1}}{\left((\sum \alpha_i)p^2 + \frac{(\sum \alpha_i)(\sum \alpha_i (p_i^2 + m_i^2)) - (\sum \alpha_i p_i)^2}{\sum \alpha_i}\right)^N}, \tag{5}$$

where

$$\Omega = \sum_{i=1}^{N} (-1)^{i-1} \alpha_i \mathrm{d}\alpha_1 \wedge \ldots \wedge \mathrm{d}\alpha_{i-1} \wedge \mathrm{d}\alpha_{i+1} \wedge \ldots \wedge \mathrm{d}\alpha_N, \tag{6}$$

and Δ is the integration region. The (one-dimensional) p-integral can be evaluated and leads to the beta-function with the result

$$\int \frac{\mathrm{d}^n p}{Q_1 \cdots Q_N} = \pi^{\frac{n}{2}} \Gamma\Big(N - \frac{n}{2}\Big) \int_\Delta \Omega \left(\sum_{i=1}^{N} \alpha_i\right)^{N-n} \left(\sum_{i,\,j=1}^{N} \alpha_i \alpha_j \frac{(p_i - p_j)^2 + m_i^2 + m_j^2}{2}\right)^{\frac{n}{2}-N}. \tag{7}$$

For the case $N = n$, the term $\left(\sum_{i=1}^{N} \alpha_i\right)^{N-n}$ becomes equal to 1 and we can just integrate over the surface

$$\Delta_1 = \left\{ \alpha_i : \sum_{i,\,j=1}^{n} \alpha_i \alpha_j \frac{(p_i - p_j)^2 + m_i^2 + m_j^2}{2} = 1,\ \alpha_i \geq 0 \right\}, \tag{8}$$

and we obtain

$$\int \mathrm{d}^n p \frac{1}{Q_1 \cdots Q_n} = \pi^{\frac{n}{2}} \Gamma\left(\frac{n}{2}\right) \int_{\Delta_1} \Omega. \tag{9}$$

Then, we do the key linear transformation to actually convert it into an area integral:

$$u^{(j)} = \sum_{i=1}^{n} \alpha_i P_i^{(j)}, \quad j = 1, \ldots, n. \tag{10}$$

This transformation in our knowledge appears explicitly for the first time in literature and is the key idea behind the motivation for the mathematical formalism in the next chapter. Here, the P_i are given by

$$P_i = p_i - c \pm ir, \tag{11}$$

with r and c satisfying

$$(p_i - c)^2 + m_i^2 = r^2, \quad i = 1, \ldots, n+1. \tag{12}$$

This follows from the sphere spanned by the momenta and masses, see Fig. 3 using which we find for their scalar products

$$\begin{aligned} P_i \cdot P_j &= (p_i - c) \cdot (p_j - c) - r^2 \\ &= \frac{(p_i - c)^2 + (p_j - c)^2 - (p_i - p_j)^2}{2} - r^2 \\ &= -\frac{(p_i - p_j)^2 + m_i^2 + m_j^2}{2}. \end{aligned} \tag{13}$$

Therefore, we can see here that the Gram determinant expression inside Eq. (8) can be conveniently expressed in terms of a dot product of two vectors. This method of expressing the Gram determinant in terms of vectors or matrices is also called as the embedding formalism in the literature. In our case, i.e., in the formalism discussed in the next subsection, we have considered c to be the origin for brevity. Due to this, the hyperbolic nature of our Feynman integral becomes evident

$$u^2 = -1. \tag{14}$$

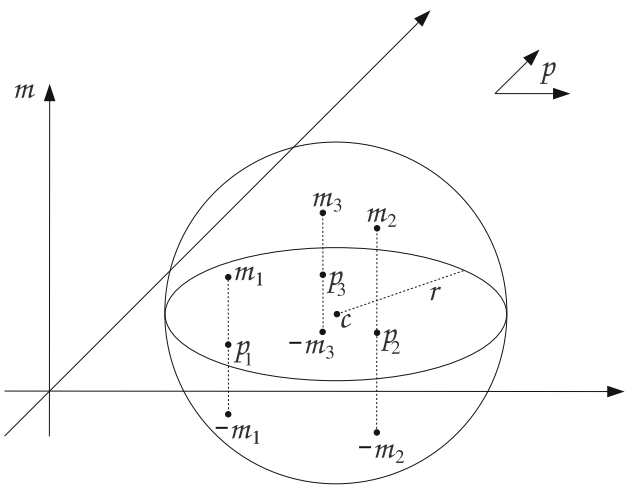

Fig. 3 The sphere spanned by the momenta and masses

This is because u^2 can be expressed in terms of $\sum_j (u^{(j)})^2$ for j dimensions in Minkowski space. The transformation Eq. (10) from the α-variables to the u-variables gives a 'Jacobian'. Altogether we obtain

$$\Omega = \frac{1}{\det(P_1^{\mathrm{M}}, \ldots, P_n^{\mathrm{M}})} \Sigma_1 \quad \text{on } \Delta_1. \tag{15}$$

Here, $\Sigma_1 = 1/u_0 \cdot \mathrm{d}u_1 \wedge \ldots \wedge \mathrm{d}u_{n-1}$. The determinant in the denominator of Eq. (15) is readily calculated:

$$\begin{aligned} &-\det(P_1^{\mathrm{M}}, \ldots, P_n^{\mathrm{M}})^2 \\ &\quad = \det\left[(P_1^{\mathrm{M}}, \ldots, P_n^{\mathrm{M}})^T \cdot \mathrm{diag}(-1, 1, \ldots, 1) \cdot (P_1^{\mathrm{M}}, \ldots, P_n^{\mathrm{M}})\right] \\ &\quad = \det\left[(P_i^{\mathrm{M}} \cdot P_j^{\mathrm{M}})_{i,j}\right] \\ &\quad = \det\left[\left(-\frac{(p_i - p_j)^2 + m_i^2 + m_j^2}{2}\right)_{i,j}\right]. \end{aligned} \tag{16}$$

Now, we can express the one-loop amplitude in terms of the volume of the $(n-1)$-dimensional hyperbolic simplex Σ spanned by $u_1^{\mathrm{M}}, \ldots, u_n^{\mathrm{M}}$

$$\int \mathrm{d}^n p \frac{1}{Q_1 \cdots Q_n} = \frac{(2\pi)^{\frac{n}{2}} \Gamma\left(\frac{n}{2}\right) \mathrm{vol}_{H^{n-1}}[\Sigma(u_1^{\mathrm{M}}, \ldots, u_n^{\mathrm{M}})]}{[(-1)^{n-1} \det((p_i - p_j)^2 + m_i^2 + m_j^2)_{i,j}]^{1/2}}. \tag{17}$$

Also, r can be expressed in terms of the momenta and masses and is given by

$$r = \left[\frac{(-1)^{n-1} \det((p_i - p_j)^2 + m_i^2 + m_j^2)_{i,j=1\ldots n}}{2^n \det((p_i - p_1) \cdot (p_j - p_1))_{i,j=2\ldots n}}\right]^{1/2}. \tag{18}$$

This can be derived from Fig. 3. And hence our main equation becomes

$$\int \mathrm{d}^n p \frac{1}{Q_1 \cdots Q_n} = \frac{\mathrm{vol}(S^n_{1/2}) \mathrm{vol}_{H^{n-1}}(\Sigma)}{r \, \mathrm{vol}_{\mathbb{R}^{n-1}}(\Sigma)}, \tag{19}$$

where $\mathrm{vol}_{H^{n-1}}(\Sigma)$ is the volume of the hyperbolic triangle and $\mathrm{vol}_{\mathbb{R}^{n-1}}(\Sigma)$ is the volume of the corresponding Euclidean triangle. In Fig. 4, the u_i variables are the vertices of the hyperbolic triangle which spans the surface $u^2 = -1$ and P_i variables are the vertices of the Euclidean triangle which spans the circular surface containing the center of the sphere. This result is purely in terms of geometrical quantities. Also, the geometrical objects

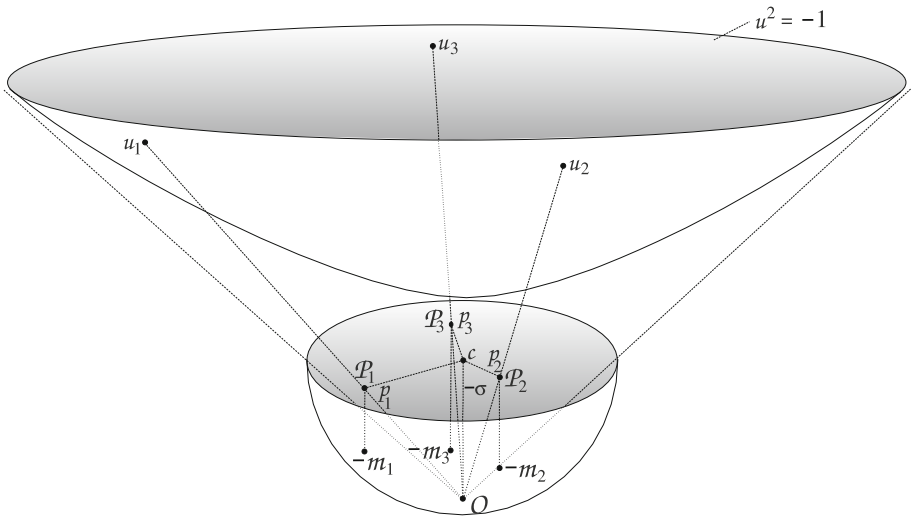

Fig. 4 Hyperbolic picture of the one-loop amplitude in Minkowski 3-space

have well-defined boundaries which paved the way for the idea of common sides. In the formalism, presented in the proceeding subsection, these geometrical objects especially the Euclidean triangle in the denominator have common sides amongst themselves which hints towards the existence of a larger geometrical structure of the whole scattering amplitude.

Note that Eq. (9) is equivalent to the representation using delta functions (see for e.g. [24])

$$\int \mathrm{d}^n p \frac{1}{Q_1 \cdots Q_n} = \pi^{\frac{n}{2}} \Gamma\left(\frac{n}{2}\right) \int_0^\infty \cdots \int_0^\infty \prod \mathrm{d}\alpha_i \times \delta\left(\sum_{i,\,j=1}^{n} \alpha_i \alpha_j \frac{(p_i - p_j)^2 + m_i^2 + m_j^2}{2} - 1\right). \tag{20}$$

This delta representation is useful in doing the calculations and can be used as a crosscheck of the formalism in [23]. Also, in the next subsection, we rewrite the expression equivalent to Eq. (9) in the representation using delta functions for crosscheck.

This sets the base for the formalism in the next subsection. We will now discuss how we extend the formalism to the whole set of one-loop Feynman diagrams contributing to the one-loop amplitude.

2.2 The main construction

2.2.1 For the $N = 3$ case

Using the result Eq. (19), we can try to add the Feynman diagrams to find out the overall geometry of the Scattering amplitudes. Here, we do the analysis for the $N = 3$ case but try to rewrite it as a general N case so that it can be easily extended to the general cases in a future work. In order to do so, we need to sum up the contributions of the tadpoles, the bubbles, and the triangle for the $N = 3$ case. The primary challenge in doing so is that using Eq. (19), the tadpoles and the bubbles will be related to a point and a line, respectively, but the triangle is associated with a triangle itself using this geometrical argument which is a two-dimensional object in contrast to the one-dimensional bubble and the zero-dimensional tadpole. Therefore, we need to construct a mathematical framework such that the bubble and the tadpole can be elevated to the space of a two-dimensional triangle.

For this, we use the property for $N = 3$ scattering the sum total of the loop propagators, and the internal propagators is always the same. For example, for the tadpole diagram, we have two internal propagators and one loop propagator (see T2, T4, and T6 in Fig. 5, the bubble has one internal propagator and two loop propagators (T3, T5, and T7) and the triangle has three loop propagators (T1) all of them having the sum total of three loop and internal propagators combined.

We rewrite the loop and internal propagators in a single framework as a part of the loop integral as follows:

$$Q_i' = (a_i p - p_i')^2 + m_i'^2, \quad i = 1, \ldots, 3N, \tag{21}$$

where

$$p_i' = \begin{cases} p_i, & i = 1, \ldots, N \\ p_{i-N,\, i-N+1}, & i = N+1, \ldots, 2N \\ 0 & i = 2N+1, \ldots, 3N, \end{cases} \tag{22}$$

and

$$a_i = \begin{cases} 1, & i = 1, \ldots, N \\ 0, & i = N+1, \ldots, 3N. \end{cases} \tag{23}$$

Here, we define the sets $I = \{i,\, i = 1,\, 2,\, ..,\, 3N\}$ and $I' \subset I$ such that there exists at least one element i in the range 1 to N and $|I'| = N$. For example, $I' = \{i = 2,\, i = 7,\, i = 9\}$ is allowed, but $I' = \{i = 4,\, i = 5,\, i = 6\}$ or $I' = \{i = 1,\, i = 2,\, i = 5,\, i = 6\}$ is not allowed for the $N = 3$ case. Thus, the range of I' covers all the Feynman integrals contributing to the one-loop scattering amplitude. The labelled Q_i' according to the above formalism is shown in Fig. 5, also see Table 1. Note that the external propagators are not included in this formalism and hence indicated by external momenta. And in place of Eq. (4), for a particular Feynman diagram in case of N particle

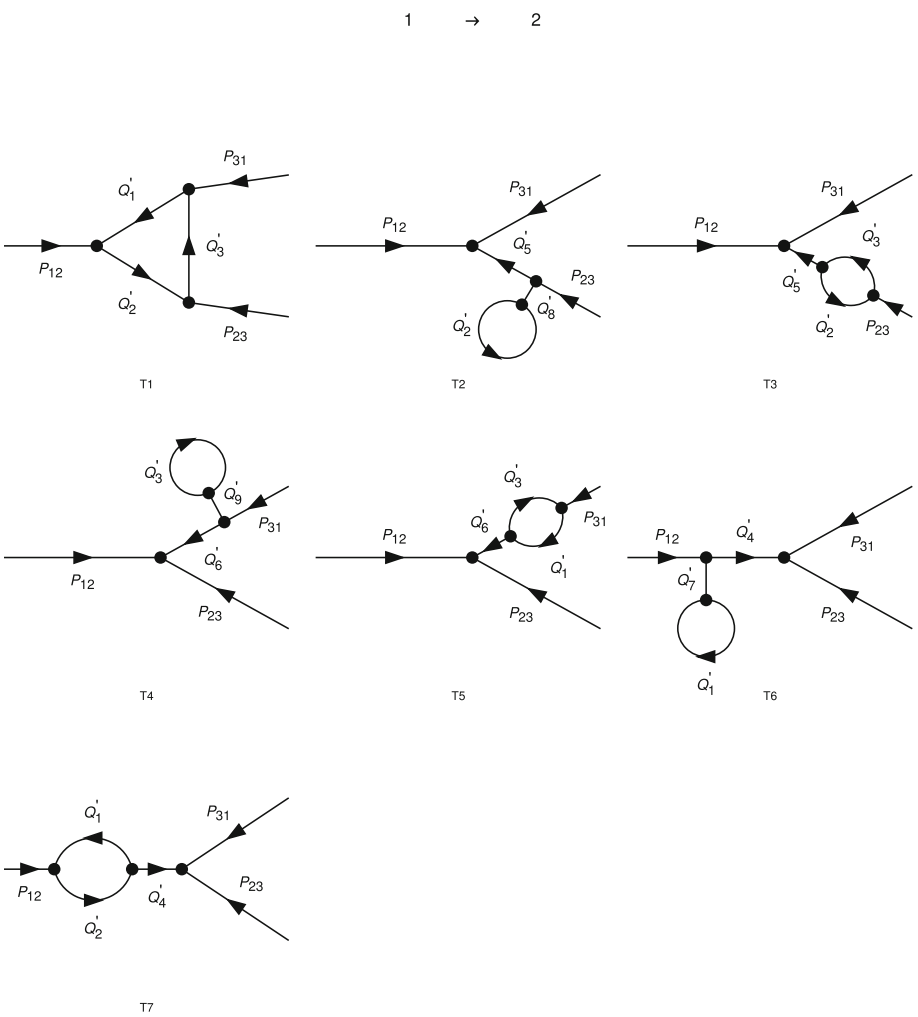

Fig. 5 $N = 3$ scattering

scattering, we have

$$\prod_{i\in I'} \frac{1}{Q_i'} = (N-1)! \int_0^\infty \prod_{i\in I'} \mathrm{d}\alpha_i \frac{\delta(1-\sum_{i\in I'}\alpha_i)}{(\sum_{i\in I'}\alpha_i Q_i')^N}. \tag{24}$$

In order to simplify the integral, we will do a similar kind of shift as we did earlier. Shifting $p \mapsto p + (\sum \alpha_i a_i p_i)/(\sum \alpha_i a_i^2)$ we get

$$\int \mathrm{d}^n p \prod_{i\in I'} \frac{1}{Q_i'} = \int_\Delta \Omega \frac{2\pi^{\frac{n}{2}}}{\Gamma(\frac{n}{2})} \int_0^\infty \frac{\mathrm{d}p\, p^{n-1}}{\left((\sum \alpha_i a_i^2)p^2 + \frac{(\sum \alpha_i a_i^2)(\sum \alpha_i (p_i'^2 + m_i'^2)) - (\sum \alpha_i a_i p_i')^2}{\sum \alpha_i a_i^2}\right)^N}. \tag{25}$$

After evaluating the p-integral, we get

$$\int \mathrm{d}^n p \prod_{i\in I'} \frac{1}{Q_i'} = \pi^{\frac{n}{2}} \Gamma\Big(N - \frac{n}{2}\Big) \int_\Delta \Omega \left(\sum_{i=1}^N \alpha_i a_i^2\right)^{N-n} \times \left(\sum_{i,j=1}^N \alpha_i \alpha_j \frac{(a_j p_i' - a_i p_j')^2 + a_j^2 m_i'^2 + a_i^2 m_j'^2}{2}\right)^{\frac{n}{2}-N}. \tag{26}$$

Again, we will consider the case $N = n$ and we are left with integrating over the surface

$$\Delta' = \left(\sum_{i,\, j=1}^{N} \alpha_i \alpha_j \frac{(a_j p'_i - a_i p'_j)^2 + a_j^2 m_i^{'2} + a_i^2 m_j^{'2}}{2} = 1,\ \ \alpha_i \geq 0 \right\}, \tag{27}$$

and thus

$$\int \mathrm{d}^n p \prod_{i \in I'} \frac{1}{Q'_i} = \pi^{\frac{n}{2}} \Gamma\left(\frac{n}{2}\right) \int_{\Delta'} \Omega. \tag{28}$$

Again, this equation is equivalent to

$$\int \mathrm{d}^n p \prod_{i \in I'} \frac{1}{Q'_i} = \pi^{\frac{n}{2}} \Gamma\left(\frac{n}{2}\right) \int_0^\infty \cdots \int_0^\infty \prod \mathrm{d}\alpha_i \delta\left(\sum_{i,\, j=1}^{N} \alpha_i \alpha_j \frac{(a_j p'_i - a_i p'_j)^2 + a_j^2 m_i^{'2} + a_i^2 m_j^{'2}}{2} - 1 \right). \tag{29}$$

Now, as in [23], in order to write the expression inside Eq. (27) as a dot product of two vectors, we will use the following equation

$$a_i^2 (m_j^{'2} + p_j^{''2}) + a_j^2 (m_i^{'2} + p_i^{''2}) = (a_i^2 + a_j^2) r_{BT}^2 + 2 a_i a_j r^2. \tag{30}$$

The definitions of r_{BT} and r alongwith the derivation of this equation is given in the appendix. Here, the momentum variables p''_i are given by

$$p_i^{''2} = \begin{cases} p_i^2, & i = 1, \ldots, N \\ (p_{i-N,\, i-N+1} - r_B)^2, & i = N+1, \ldots, 2N \\ r_{BT}^2 - m_i^{'2} & i = 2N+1, \ldots, 3N, \end{cases} \tag{31}$$

where r_B is also defined in the appendix. Using this, we get

$$\begin{aligned} &\frac{(a_j p''_i - a_i p''_j)^2 + a_j^2 m_i^{'2} + a_i^2 m_j^{'2}}{2} \\ &= \left[a_j p''_i - i a_j \left(\sqrt{r^2 + r_{BT}^2} \right) \right] \cdot \left[a_i p''_j - i a_i \left(\sqrt{r^2 + r_{BT}^2} \right) \right] + \frac{(a_i - a_j)^2 r_{BT}^2}{2}. \end{aligned} \tag{32}$$

Here, we have chosen $c = 0$ in Eq. (34) of [23] which according to the explanation there is arbitrary. Therefore, here, we get the momentum variables shifted for the case $a_i = 0$ and hence the actual value of the bubble and tadpole propagators also gets shifted to r_{BT}^2!. In order to deal with this, we will add the following term to both the sides of Eq. (32)

$$\frac{-(a_i^2 + a_j^2) r_{BT}^2 + a_i^2 r_j^2 + a_j^2 r_i^2}{2},$$

which gives

$$\begin{aligned} &\frac{(a_j p''_i - a_i p''_j)^2 + a_j^2 m_i^{'2} + a_i^2 m_j^{'2} - (a_i^2 + a_j^2) r_{BT}^2 + a_i^2 r_j^2 + a_j^2 r_i^2}{2} \\ &= \frac{(a_j p'_i - a_i p'_j)^2 + a_j^2 m_i^{'2} + a_i^2 m_j^{'2}}{2} \\ &= \left[a_j p''_i - i a_j \left(\sqrt{r^2 + r_{BT}^2} \right) \right] \cdot \left[a_i p''_j - i a_i \left(\sqrt{r^2 + r_{BT}^2} \right) \right] - a_i a_j r_{BT}^2 + \frac{a_i^2 r_j^2 + a_j^2 r_i^2}{2}, \end{aligned} \tag{33}$$

where r_i and r_j are once again defined in appendix. Therefore, the LHS of this equation when traced back gives the original value of the propagators. Thus, if we define the new linear transformation, here it will be

$$v^{(k)} = \sum_{i,\,j=1}^{n} \alpha_j \left[a_i p_j'' - i a_i R\right]^{(k)}, \quad k = 1, \ldots, n, \tag{34}$$

where

$$R = \sqrt{r^2 + r_{BT}^2}. \tag{35}$$

Now, if we define a inner product to be of the form (it is also called the Frobenius inner product)

$$\langle v|v\rangle = u'^2 = \sum_{i,\,j=1}^{n} \alpha_i \alpha_j [a_i p_i'' - i a_i R] \cdot \left[a_j p_j'' - i a_j R\right], \tag{36}$$

where

$$u'^{(k)} = \sum_{i=1}^{n} \alpha_i [a_i p_i'' - i a_i R]^{(k)}, \quad k = 1, \ldots, n, \tag{37}$$

is equivalent to the u defined in [23]. The significance behind defining two different type of vectors v and u' will be explained in a while. Now, if

$$P'_{ij} = \left[a_i p_j'' - i a_i R)\right], \tag{38}$$

we have

$$\langle v|v\rangle = u'^2 = \sum_{i,\,j=1}^{n} \alpha_i \alpha_j P'_{ii} \cdot P'_{jj} = -1 + \sum_{i,\,j=1}^{n} \alpha_i \alpha_j \left[a_i a_j r_{BT}^2 - \frac{a_i^2 r_j^2 + a_j^2 r_i^2}{2}\right]. \tag{39}$$

then we get a similar kind of situation as in [23] but this time the normal inner product getting converted to Frobenius product if we consider the v variables and along with a additional shift term as seen in the RHS of the above equation. Here, Eq. (39) represents a general quadric surface equation where the hyperbolic geometry of [23] is a special case of this general quadric surface geometry as we will see in the next section. Here, we have the spanning Minkowski space vectors given by

$$v_j^{\mathrm{M}} = \left(\sum_{i=1}^{n} P_{ij}'^{\mathrm{M}}\right) / \sum_{i=1}^{n} a_i m'_j, \tag{40}$$

with

$$P_{ij}'^{\mathrm{M}} = (a_i R,\, a_i p_j''^{M}), \tag{41}$$

and

$$\left(\sum_{i=1}^{n} P_{ij}'^{\mathrm{M}}\right)^2 = -\sum_{i=1}^{n} a_i^2 m_j'^2. \tag{42}$$

Thus, following similar steps as in [23] finally Eq. (28) becomes

$$\int \mathrm{d}^n p \prod_{i \in I'} \frac{1}{Q'_i} = \frac{\mathrm{vol}(S^n_{1/2}) \mathrm{vol}_{C^{n-1}}(\Sigma(v_i^{\mathrm{M}}))}{R\, \mathrm{vol}_{\mathbb{R}^{n-1}}(\Sigma(p_i^{\mathrm{M}}))(\sum_i a_i)^n}. \tag{43}$$

Here, C^{n-1} represents the general quadric surface geometry in $n-1$ dimensions. In the following sections, we will see what type of geometry it leads to for different cases. Note that there is a $\sum_i a_i$ term in the denominator because in the change of variables linear transformation we have chosen the v_i variables which have this factor

inside them. If we would have chosen the u_i' variables, then it would have been a product of all a_i i.e. $\prod_i a_i$. This is the reason we have to define a different set of variables v other than u'.

As we said, the factor$\sum_i a_i$ is inside and can be taken out common from the v_i variables. Therefore, first of all, we rewrite Eq. (34) as

$$v^{(k)} = \left(\sum_{i=1}^{n} a_i\right) \sum_{j=1}^{n} \alpha_j \left[p_j'' - iR\right]^{(k)}, \quad k = 1, \ldots, n. \tag{44}$$

We can make the calculations simpler by defining

$$v'^{(k)} = \frac{v^{(k)}}{(\sum_{i=1}^{n} a_i)} = \sum_{j=1}^{n} \alpha_j \left[p_j'' - iR\right]^{(k)}, \quad k = 1, \ldots, n, \tag{45}$$

because of which Eq. (43) takes the form

$$\int \mathrm{d}^n p \prod_{i \in I'} \frac{1}{Q_{i'}} = \frac{\mathrm{vol}(S^n_{1/2}) \mathrm{vol}_{C^{n-1}}(\Sigma({v_i}'^{\mathrm{M}}))}{R\, \mathrm{vol}_{\mathbb{R}^{n-1}}(\Sigma(p_i''^{\mathrm{M}}))}. \tag{46}$$

Thus, this mathematical framework has put the bubbles and the tadpoles on the same footing as the triangle and using this equation we can construct an Euclidean triangle and a corresponding quadric triangle corresponding to each diagram in Fig. 5 as follows.

2.2.2 Singularity analysis

In this section, we will talk about potential divergence problems that might arise from the new formalism and possible ways to counter them. As pointed out above, the choice of variables eliminates the possibility of singularities in Eq. (46) due to the vanishing of one or more $a_i's$. This will be more clear with the analysis given in the proceeding sections. In addition to this, generally Feynman integrals also suffer from singularities after performing the loop integral which appears in the final analytic expressions for their results usually in the form of singularities of the gamma function, see [27, 28]. Here, the analytic result for the one-loop $N-$ point Feynman integral is given by

$$\begin{aligned} I^{(N)}(m_1, \ldots, m_N) = {} & \pi^{n/2} i^{1-n} (-m_N^2)^{n/2-N} \frac{\Gamma(N - n/2)}{\Gamma(N)} \\ & \times F_D^{(N-1)}\left(N - \frac{n}{2}, 1, \ldots, 1; N \mid 1 - \frac{m_1^2}{m_N^2}, \ldots, 1 - \frac{m_{N-1}^2}{m_N^2}\right), \end{aligned} \tag{47}$$

where $F_D^{(L)}$ represents the Lauricella function of $L-$variables given by

$$\begin{aligned} & F_D^{(L)}(a, b_1, \ldots, b_L; c \mid z_1, \ldots, z_L) \\ & = \sum_{j_1=0}^{\infty} \cdots \sum_{j_L=0}^{\infty} \frac{(a)_{j_1+\cdots+j_L} (b_1)_{j_1} \cdots (b_L)_{j_L}}{(c)_{j_1+\cdots+j_L}} \times \frac{z_1^{j_1} \cdots z_L^{j_L}}{j_1! \cdots j_L!}. \end{aligned} \tag{48}$$

From the above, it may be seen that the triangle, bubble and tadpole will escape any singularity arising from the arguments of the gamma functions in $n = 3$ dimensions, though they will become divergent for $n = 4$ and most probably can be solved using dimensional regularisation which ultimately becomes the subject of future investigations. Also, any other hidden singularities arising due to the Lauricella functions is a matter of ongoing work.

Also, for the case when one or more of the masses go to zero, then the function $F_D^{(N-1)}$ reduces to $F_D^{(N-2)}$, using the following relation, see [27], which can be easily extended to the vanishing of multiple masses case

$$\begin{aligned} F_D^{(L)}(a, b_1, \ldots, b_{L-1}, b_L; c \mid z_1, \ldots, z_{L-1}, 1) = {} & \frac{\Gamma(c)\Gamma(c - a - b_L)}{\Gamma(c - a)\Gamma(c - b_L)} \\ & \times F_D^{(L-1)}(a, b_1, \ldots, b_{L-1}; c - b_L \mid z_1, \ldots, z_{L-1}). \end{aligned} \tag{49}$$

From the above, it may be seen that we get the similar form of the arguments of the gamma function and hence consequently the same conditions for singularities. Finally, one more possibility of divergence arises when the volume function in the denominator of Eq. (46) vanishes. This may happen if the two of the momenta become collinear. In this case, the volume function in the numerator will also go to zero and we may get the final result finite which can be evaluated if we evaluate the functions in a dimension lower by one, e.g., evaluating the length instead of evaluating the area for the present $n = 3$ case.

2.3 Construction of the triangles in mapped space

We want to see what features the triangles represent when we map the Feynman integrals to them according to this new mathematical formalism. In [23], the triangle diagram T1 in Fig. 5 is mapped to a triangle using the linear transformation defining the vector u_i but with p_i momenta being the position vectors for the vertices instead of being inside the loop propagator. The original triangle Feynman diagram has no notion of a side length, but here side length and the shape of the mapped triangle are important. Using the formalism presented in this paper, specifically the linear transformation in Eq. (45), we can map the other types of Feynman diagrams like the bubbles (T3,T5,T7) and the tadpoles (T2,T4,T6) but with different shapes and side lengths.

2.3.1 Without the shifts

We will draw the mapped triangles now using Eq. (45) but first with p_i' defined in Eq. (22) instead of p_i'' defined in Eq. (31) for brevity and as a first step in understanding. A table, Table 1, is provided in the appendix relating the diagrams with the corresponding Q_i, v_i and p_i. In the next subsection, we will do it for the actual value p_i''. If we denote the incoming momentum in Fig. 5 as p_{12} and the outgoing momenta as p_{23} and p_{31} then the three vertices of T1 correspond to vectors p_1, p_2 and p_3. For T2, there are two internal propagators with momenta p_{23} and zero, and one loop propagator with momenta p_2 so the corresponding triangles will have vertices p_{23}, origin (0) and p_2. In this way, we can construct all the triangles in Fig. 6. Also, here, we have taken the random example $p_1 = \{-1, 2\}$, $p_2 = \{-2, -2\}$ an $p_3 = \{4, 0\}$ with $O = \{0, 0\}$ as origin for illustration.

So here, we can see that all the triangles have a common side. For example, T1 and T2 have a common side ($p_2 - p_3$ and $O - p_{23}$),T2 and T3 have a common side ($p_2 - p_{23}$), T1 and T4 have a common side ($p_3 - p_1$ and $O - p_{31}$) and so on. This is the main result of our paper to show that using our formalism, we can map the Feynman diagrams to triangles having common sides.

2.3.2 With shifts

We can do the same thing as above now with p_i'', which gives the original value of propagators. In Eq. (31), for $i = 2N + 1, \ldots, 3N$, the magnitude of p_i'' is clear, but the direction is arbitrary. It can be fixed if we follow a particular convention which dictates that p_i and p_{2N+i} become parallel to each other. This specific convention does the precious job of simplifying the calculations and yields the most compact result possible. We have given a detailed discussion about this in Sect. 5.

After drawing the mapped triangles using Eq. (45), we see that we still have one side common between triangles, see Fig. 7. For example, T1 and T3 have a common side ($p_2 - p_3$), T2 and T3 have a common side ($p_2 - p_{23} - r_B$), T1 and T5 have a common side ($p_1 - p_3$) and so on. Here, we have taken $r_B = \{0, 1\}$ and $p_{2N+i} = p_i/2$. Therefore, once again, our main argument of showing triangles with common sides is satisfied.

3 The general quadric surface equation for different cases

Now, in order to evaluate Eq. (46), we need to find out the volume of the conic simplex $\Sigma(v_i^{\mathrm{M}})$ which is obtained by the intersection of the cone spanned by $\sum_i P_{ij}'$ and the surface governed by Eq. (46).

For this, we need to find out how to express the general quadric surface equation in terms of the vectors $v^{'(k)}$ in Eq. (45). This can be done by first expressing the $\alpha_i' s$ in terms of these vectors and then substituting in Eq. (36).

Equation (45) represents a matrix equation and can be solved by taking the inverse [29]:

$$\alpha_j = \sum_{k=1}^{n} \frac{\varepsilon_{j_1 \ldots j_{n-1} j} \varepsilon_{k_1 \ldots k_{n-1} k} v^{'(k)}}{(n-1)! \det(p_1'' - iR, .., p_n'' - iR)} \prod_{l=1}^{n-1} \left[p_{j_l}'' - iR\right]^{(k_l)}, \quad j = 1, \ldots, n, \tag{50}$$

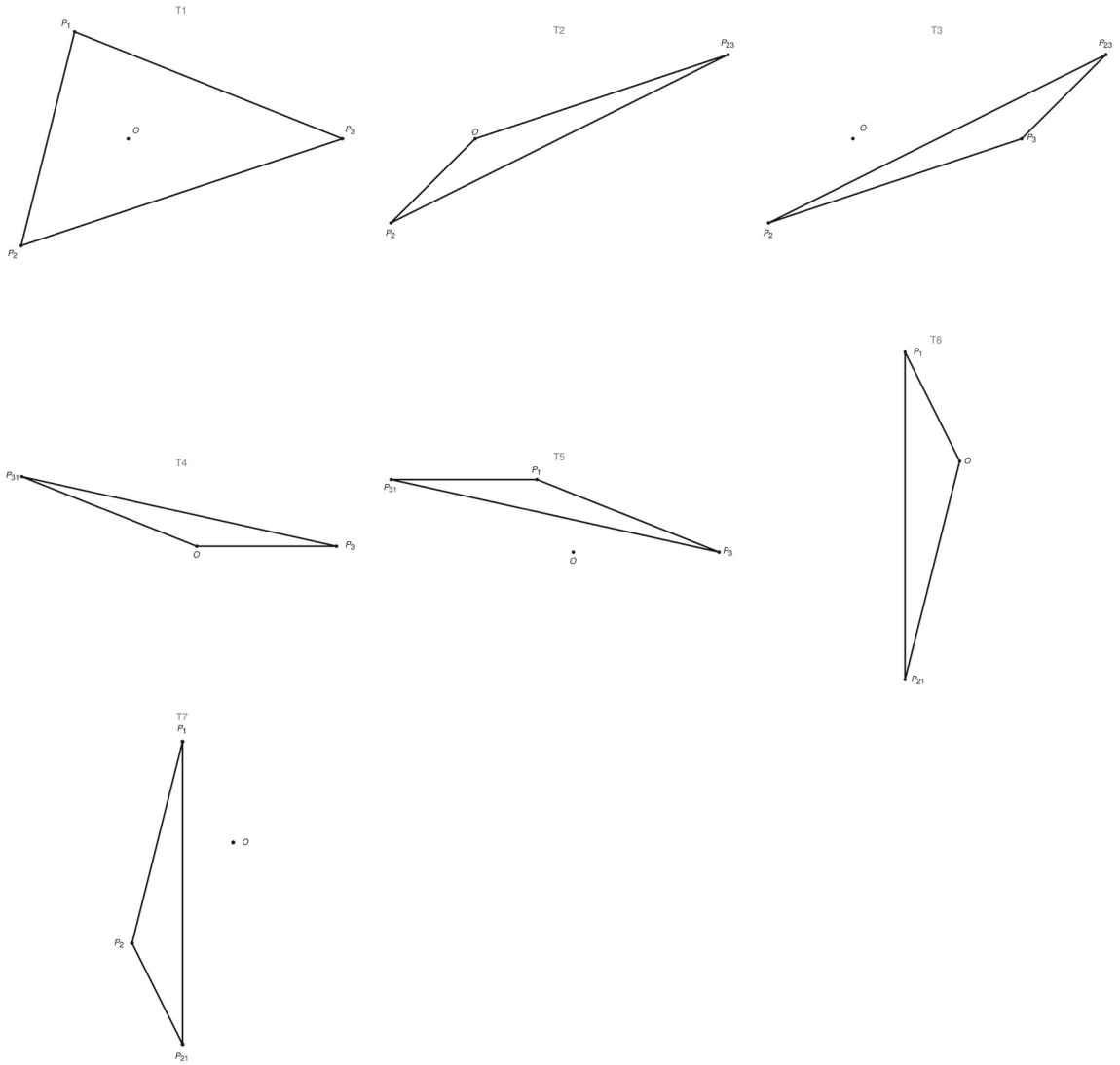

Fig. 6 Triangles without shift

where ε are the generalized Levi-Civita tensors and Einstein summation convention is implied for the j_l and k_l indices. Now, using Eqs. (36) and (45), Eq. (39) can be rewritten in a matrix form as

$$\begin{aligned}
&\Big[\alpha_1[p_1''-iR]\ \alpha_2[p_2''-iR]\cdots\alpha_n[p_n''-iR]\Big]\begin{bmatrix} a_1^2 & a_1a_2 & \cdots & a_1a_n \\ a_1a_2 & a_2^2 & \cdots & a_2a_n \\ \vdots & \vdots & \ddots & \vdots \\ a_1a_n & a_2a_n & \cdots & a_n^2 \end{bmatrix}\begin{bmatrix} \alpha_1[p_1''-iR] \\ \alpha_2[p_2''-iR] \\ \vdots \\ \alpha_n[p_n''-iR] \end{bmatrix} \\
&= -1+\Big[\alpha_1\ \alpha_2\cdots\alpha_n\Big]\left\{\begin{bmatrix} a_1^2 & a_1a_2 & \cdots & a_1a_n \\ a_1a_2 & a_2^2 & \cdots & a_2a_n \\ \vdots & \vdots & \ddots & \vdots \\ a_1a_n & a_2a_n & \cdots & a_n^2 \end{bmatrix}-\begin{bmatrix} a_1^2r_1^2 & a_1^2r_2^2 & \cdots & a_1^2r_n^2 \\ a_2^2r_1^2 & a_2^2r_2^2 & \cdots & a_2^2r_n^2 \\ \vdots & \vdots & \ddots & \vdots \\ a_n^2r_1^2 & a_n^2r_2^2 & \cdots & a_n^2r_n^2 \end{bmatrix}\right\}\begin{bmatrix} \alpha_1 \\ \alpha_2 \\ \vdots \\ \alpha_n \end{bmatrix},
\end{aligned} \tag{51}$$

where the $\alpha_i's$ are given by Eq. (50). Note that the last term inside the square bracket in Eq. (39) is actually symmetric and hence only one of its parts is written here by dropping the half factor. This is the general quadric

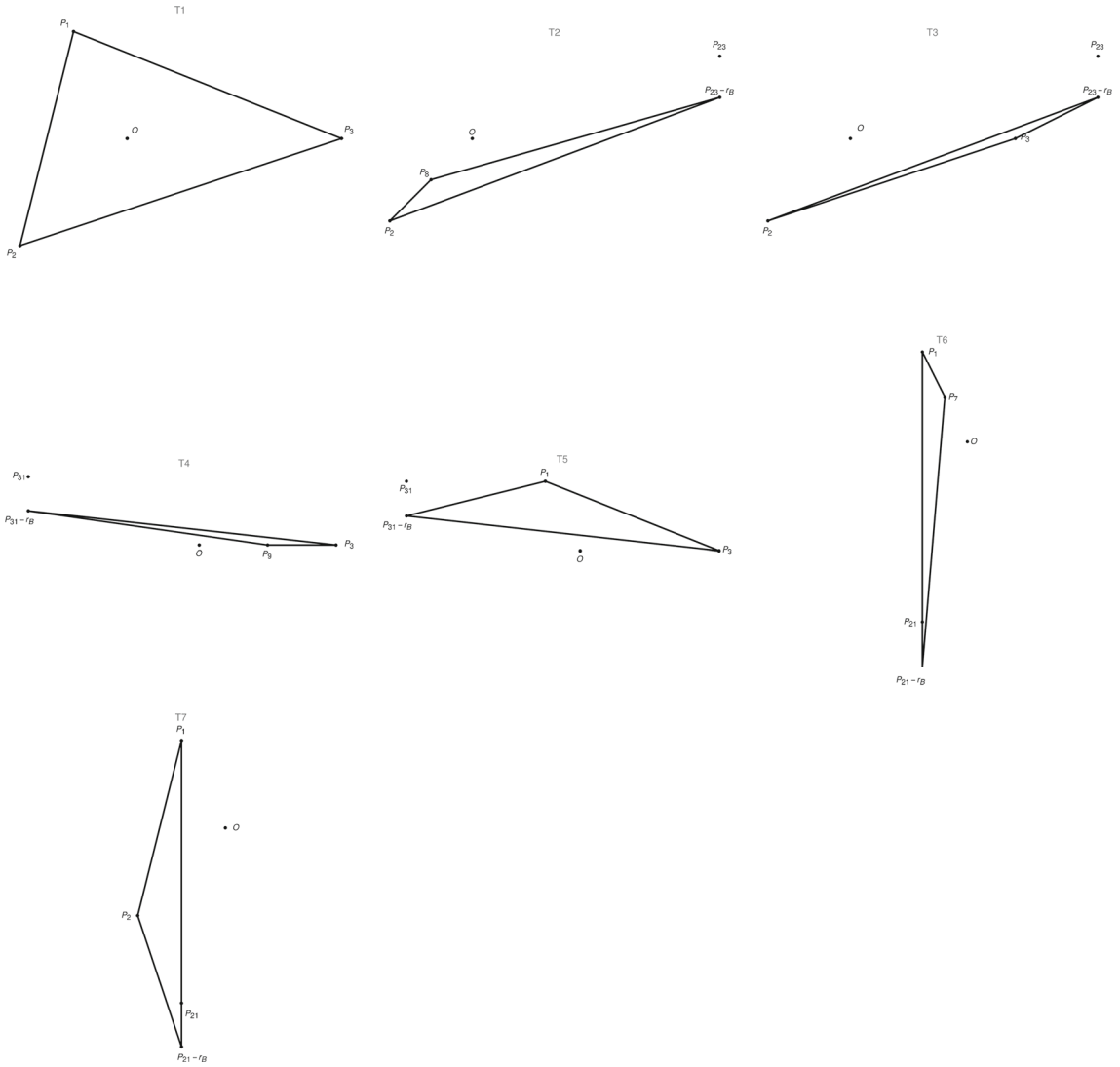

Fig. 7 Triangles with shift

surface equation which can be plotted in terms of $v^{'(k)}$. And for finding out the the principal axes of the general quadric surface, we need to diagonalize the set of middle matrices in LHS of the above equation with components of v' as elements in the row and column matrix at the right and left sides of the set of middle matrices, respectively.

Diagonalize this

$$\begin{bmatrix} v^{'(1)} & v^{'(2)} & \cdots & v^{'(n)} \end{bmatrix}$$

$$\overbrace{\left\{\begin{bmatrix} \alpha_1^{'(1)}[p_1''-iR] & \alpha_2^{'(1)}[p_2''-iR] & \cdots & \alpha_n^{'(1)}[p_n''-iR] \\ \alpha_1^{'(2)}[p_1''-iR] & \alpha_2^{'(2)}[p_2''-iR] & \cdots & \alpha_n^{'(2)}[p_n''-iR] \\ \vdots & \vdots & \ddots & \vdots \\ \alpha_1^{'(n)}[p_1''-iR] & \alpha_2^{'(n)}[p_2''-iR] & \cdots & \alpha_n^{'(n)}[p_n''-iR] \end{bmatrix}\begin{bmatrix} a_1^2 & a_1a_2 & \cdots & a_1a_n \\ a_1a_2 & a_2^2 & \cdots & a_2a_n \\ \vdots & \vdots & \ddots & \vdots \\ a_1a_n & a_2a_n & \cdots & a_n^2 \end{bmatrix}\begin{bmatrix} \alpha_1^{'(1)}[p_1''-iR] & \alpha_2^{'(1)}[p_2''-iR] & \cdots & \alpha_n^{'(1)}[p_n''-iR] \\ \alpha_1^{'(2)}[p_1''-iR] & \alpha_2^{'(2)}[p_2''-iR] & \cdots & \alpha_n^{'(2)}[p_n''-iR] \\ \vdots & \vdots & \ddots & \vdots \\ \alpha_1^{'(n)}[p_1''-iR] & \alpha_2^{'(n)}[p_2''-iR] & \cdots & \alpha_n^{'(n)}[p_n''-iR] \end{bmatrix}^T}$$

$$\underbrace{-\begin{bmatrix} \alpha_1^{'(1)} & \alpha_2^{'(1)} & \cdots & \alpha_n^{'(1)} \\ \alpha_1^{'(2)} & \alpha_2^{'(2)} & \cdots & \alpha_n^{'(2)} \\ \vdots & \vdots & \ddots & \vdots \\ \alpha_1^{'(n)} & \alpha_2^{'(n)} & \cdots & \alpha_n^{'(n)} \end{bmatrix}\left\{\begin{bmatrix} a_1^2 & a_1a_2 & \cdots & a_1a_n \\ a_1a_2 & a_2^2 & \cdots & a_2a_n \\ \vdots & \vdots & \ddots & \vdots \\ a_1a_n & a_2a_n & \cdots & a_n^2 \end{bmatrix}-\begin{bmatrix} a_1^2r_1^2 & a_1^2r_2^2 & \cdots & a_1^2r_n^2 \\ a_2^2r_1^2 & a_2^2r_2^2 & \cdots & a_2^2r_n^2 \\ \vdots & \vdots & \ddots & \vdots \\ a_n^2r_1^2 & a_n^2r_2^2 & \cdots & a_n^2r_n^2 \end{bmatrix}\right\}\begin{bmatrix} \alpha_1^{'(1)} & \alpha_2^{'(1)} & \cdots & \alpha_n^{'(1)} \\ \alpha_1^{'(2)} & \alpha_2^{'(2)} & \cdots & \alpha_n^{'(2)} \\ \vdots & \vdots & \ddots & \vdots \\ \alpha_1^{'(n)} & \alpha_2^{'(n)} & \cdots & \alpha_n^{'(n)} \end{bmatrix}^T}_{}\begin{bmatrix} v^{'(1)} \\ v^{'(2)} \\ \vdots \\ v^{'(n)} \end{bmatrix} = -1, \tag{52}$$

where

$$\alpha_j^{'(k)} = \frac{\varepsilon_{j_1 \ldots j_{n-1} j} \varepsilon_{k_1 \ldots k_{n-1} k}}{(n-1)! \det(p_1'' - iR, .., p_n'' - iR)} \prod_{l=1}^{n-1} \left[p_{j_l}'' - iR\right]^{(k_l)}, \quad j = 1, \ldots, n. \tag{53}$$

The diagonalization can be performed by using spectral decomposition where the diagonalizable matrix A can be written as a product of unitary matrix U, diagonal matrix D, and the transpose of the unitary matrix

$$A = UDU^T, \tag{54}$$

where D is the diagonal matrix comprising of the eigenvalues of A and U is the orthonormal eigenvector basis with corresponding eigenvectors as columns of U. Therefore, if the eigenvalues are given by λ_i and the column vectors of U are given by u_i then the general quadric surface becomes [30]

$$\lambda_1 (u_1.v')^2 + \lambda_2 (u_2.v')^2 + \cdots + \lambda_n (u_n.v')^2 = -1. \tag{55}$$

Thus, the principal axes of the general quadric surface lie in the direction of u_i, and if we choose one of the directions to have the complex part of the momenta (iR), for example, if we choose u_1, then using Eq. (55), we can see that the general quadric surface actually satisfies hyperbolic geometry with unequal eigenvalues.

This is different from the situation in [23] in the way that the principal axes of the hyperbolic geometry there was parallel to coordinate axes, and the eigenvalues were of equal magnitude unity. Here, the principal axes with different magnitudes of eigenvalues are rotated with respect to the coordinate axes in the case of one or more $a_i = 0$.

Now, here we have three cases of the general quadric surface, Eq. (55), as per the type of corresponding Feynman diagram—the triangle, the bubbles, and the tadpoles.

3.1 Triangle

For the triangle case, we have all $a_i's = 1$ and hence using Eqs. (45) and (51), the general quadric surface equation becomes

$$v^{'2} = -1. \tag{56}$$

For $n = 3$, if we choose the complex part of momenta (iR) to be in the $v^{'(3)}$ direction, then this denotes the equation of hyperboloid of two sheets, see Fig. 8

$$(v^{'(1)})^2 + (v^{'(2)})^2 - (v^{'(3)})^2 = -1. \tag{57}$$

Therefore, this is a special case where the eigenvalues are equal in magnitude in the general quadric surface equation Eq. (55). Now, according to Eq. (43), we have to find out the volume of the intersection region of the infinite open simplex made by p_i' vectors and the above surface.

3.2 Bubble

We get a bubble diagram when any two out of three $a_i's = 1$ and the third one equals zero. Therefore, in Eq. (51), the middle matrix is block diagonal for this case, with any one diagonal entry equal to zero. Because of this, it is not very hard to infer that the eigenvalue matrix D will also be block diagonal in this case, with the corresponding eigenvalue equal to zero. A proof of this has been given in the appendix.

Using this Eq. (55) roughly becomes of the form

$$-\lambda_1 (u_1.v')^2 + \lambda_2 (u_2.v')^2 + \cdots + \lambda_{n-1} (u_{n-1}.v')^2 + 0.(u_n.v')^2 = -1. \tag{58}$$

where the complex part of momenta (iR) is chosen along u_1 direction, and the nth eigenvalue is chosen to be zero. Here, we can see that this equation for $n = 3$ pertains to the equation of elliptic hyperboloid of two sheets but with one of the axes of the ellipse having length equal to infinity $(1/\sqrt{\lambda_n} = \infty)$. Therefore, this looks like a hyperbolic cylinder, see Fig. 9.

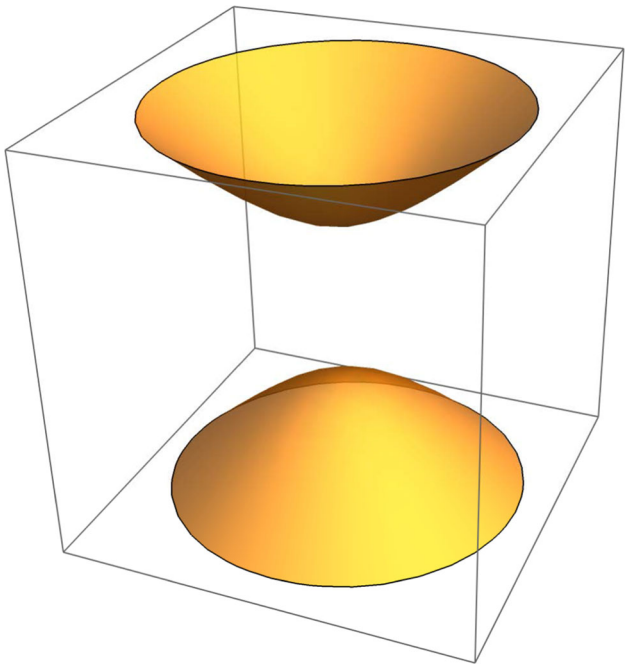

Fig. 8 Hyperboloid of two sheets

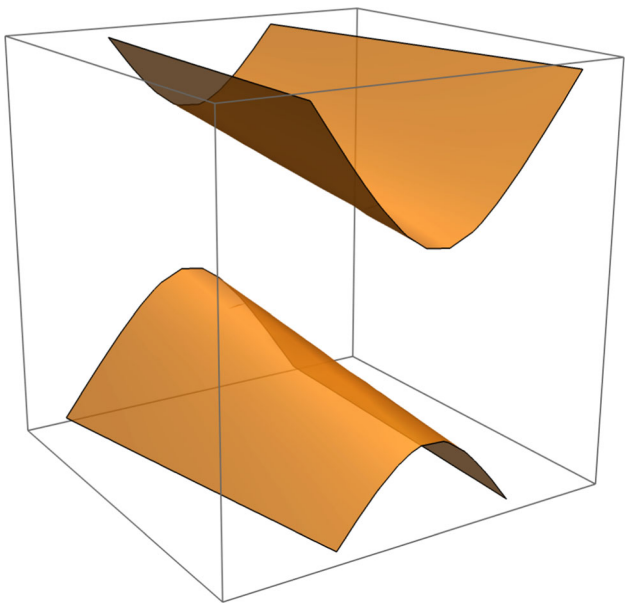

Fig. 9 Hyperboloid of two sheets with one flat axis

3.3 Tadpole

Now for the tadpole case, any two out of three $a_i's$ are equal to zero, and the third one is equal to one. Due to this, once again, the middle matrix in Eq. (51) is block diagonal with any two diagonal entries equal to zero. Again due to this, the eigenvalue matrix D becomes block diagonal with any two corresponding eigenvalues equal to zero.

$$-\lambda_1(u_1.v')^2 + \lambda_2(u_2.v')^2 + \cdots + \lambda_{n-2}(u_{n-2}.v')^2 + 0.(u_{n-1}.v')^2 + 0.(u_n.v')^2 = -1. \tag{59}$$

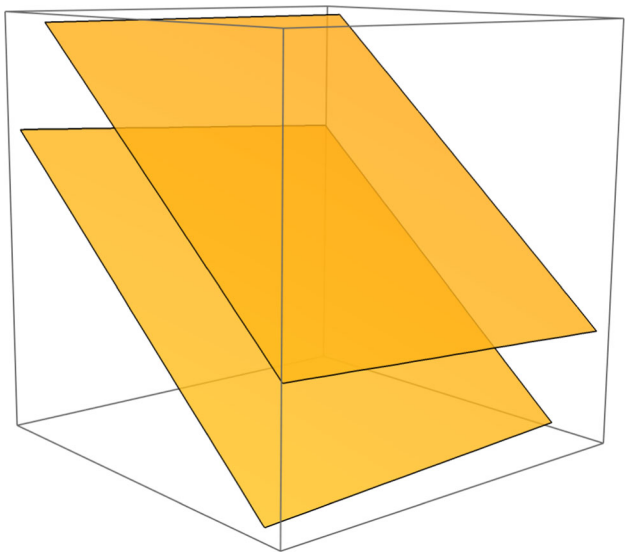

Fig. 10 Hyperboloid of two sheets with both flat axis

So for the $n = 3$ case, this is still the equation for the elliptic hyperboloid but with both the ellipse axes having length equal to infinity. Therefore, the cup of the hyperboloid completely flattens down, and what we get are just two completely flat planes, see Fig. 10.

4 Evaluation of the Feynman diagrams

Now, the Feynman diagram can be evaluated from the obtained quadrics by finding out the volume of intersection of the quadric with corresponding simplex made by the $p_i'' - iR$ vectors.

For this, we need to first find out the volume element $vol_{C^{n-1}}(\Sigma(v_i'^{\mathrm{M}}))$ in Eq. (46). Using Eq. (55) for the $n = 3$ case, it is given by

$$vol_{C^{n-1}}(\Sigma(v_i'^{\mathrm{M}})) = \int \delta\big(\lambda_1(u_1.v')^2 + \lambda_2(u_2.v')^2 + \lambda_3(u_3.v')^2 + 1\big) dv'^{(1)} dv'^{(2)} dv'^{(3)}. \tag{60}$$

If we do the $v'^{(3)}$ integration first and if $u_j^{(i)}$ is the component of u_j along the direction of $v'^{(i)}$, then we get

$$vol_{C^{n-1}}(\Sigma(v_i'^{\mathrm{M}})) = \int dv'^{(1)} dv'^{(2)} \left(\left(\sum_i \lambda_i \left(u_i^{(3)} \right)^2 \right) \left(\sum_i \lambda_i \left(\sum_j u_i^{(j)} v'^{(j)} \right)^2 \right. \right.$$
$$\left. \left. - \left(\sum_i \lambda_i u_i^{(3)} \left(\sum_j u_i^{(j)} v'^{(j)} \right) \right)^2 \left(\sum_i \lambda_i \left(u_i^{(3)} \right) \right)^{-1} + 1 \right) \right)^{-1}. \tag{61}$$

Now, this can be solved using polar co-ordinates

$$v'^{(1)} = \rho \cos\theta \tag{62}$$

$$v'^{(2)} = \rho \sin\theta, \tag{63}$$

where ρ is the radial distance from the origin and θ is the usual angle in polar co-ordinates. Using this eq.(61) becomes

$$vol_{C^{n-1}}(\Sigma(v_i'^{\mathrm{M}})) = \int \frac{\rho\, d\rho\, d\theta}{\sqrt{A[u_i](\rho^2 C[\theta]+1)}}, \tag{64}$$

where

$$A[u_i] = \left(\sum_i \lambda_i \left(u_i^{(3)}\right)^2\right) \tag{65}$$

$$\rho^2 C[\theta] = \sum_i \lambda_i \left(\sum_j u_i^{(j)} v'^{(j)}\right)^2 - \left(\sum_i \lambda_i u_i^{(3)} \left(\sum_j u_i^{(j)} v'^{(j)}\right)\right)^2 \left(\sum_i \lambda_i \left(u_i^{(3)}\right)\right)^{-1}. \tag{66}$$

Now if we define

$$\gamma = \frac{\rho}{v'^{(3)}} = \rho\left(\rho B[\theta] + \sqrt{-\frac{\rho^2 C[\theta]+1}{A[u_i]}}\right)^{-1}, \tag{67}$$

with

$$\rho B[\theta] = -\left(\sum_i \lambda_i u_i^{(3)} \left(\sum_j u_i^{(j)} v'^{(j)}\right)\right), \tag{68}$$

then the integral becomes

$$vol_{C^{n-1}}(\Sigma(v_i'^{\mathrm{M}})) = \int \frac{\sqrt{A[u_i]}\gamma(\gamma B[\theta]-1)}{(A[u_i](\gamma B[\theta]-1)^2+\gamma^2 C[\theta])^2} \sqrt{-\frac{\gamma^2 C[\theta]}{A[u_i](\gamma B[\theta]-1)^2}-1}\; d\gamma d\theta. \tag{69}$$

The geometrical significance of the variable γ will be described in the following subsections. The γ integration can be made in a straightforward manner and the result is given by

$$vol_{C^{n-1}}(\Sigma({v_i}'^{\mathrm{M}})) = \int -\frac{\frac{1}{\sqrt{-\frac{a^2 b^2 C[\theta]}{A[u_i](\csc(\theta 2)(b\sin(\theta-\theta 1-\theta 2)-a\sin(\theta-\theta 1))+abB[\theta])^2}-1}}+i}{\sqrt{A[u_i]C[\theta]}} d\theta. \tag{70}$$

The limits of this integration have been discussed in detail in the following subsection. The θ integration is difficult, and we can get a solution in terms of infinite sums of known functions. This is not actually required for the time being, and hence we will just take a series expansion of Eq. (69) and then do the integration. Therefore, if we do this, we get

$$\begin{aligned} vol_{C^{n-1}}(\Sigma(v_i'^{\mathrm{M}})) = \int \mathrm{d}\gamma d\theta \Bigg\{ & -\frac{i\gamma}{(A[u_i])^{3/2}} - \frac{3i\gamma^2 B[\theta]}{(A[u_i])^{3/2}} - \frac{5i\gamma^4\left(4A[u_i]b_\theta^3 - 3B[\theta]C[\theta]\right)}{2(A[u_i])^{5/2}} - \frac{3i\gamma^3\left(4A[u_i]B[\theta]^2 - C[\theta]\right)}{2(A[u_i])^{5/2}} \\ & - \frac{15i\gamma^5\left(8(A[u_i])^2 B[\theta]^4 - 12A[u_i]B[\theta]^2 C[\theta] + C[\theta]^2\right)}{8(A[u_i])^{7/2}} + \cdots. \end{aligned} \tag{71}$$

Now, this can be solved order by order in γ. We have discussed the evaluation for different cases in the following subsections.

4.1 Triangle

For the triangle, we inferred that the quadric is actually a hyperboloid of two sheets with principal axis parallel to the axis containing the complex part of the momenta. Hence, using Eq. (57), the $vol_{C^{n-1}}(\Sigma(v_i^{'M}))$ in Eq. (46) takes the form

$$vol_{C^{n-1}}(\Sigma(v_i^{'M})) = \int \delta\Big((v^{'(1)})^2 + (v^{'(2)})^2 - (v^{'(3)})^2 + 1\Big) dv^{'(1)} dv^{'(2)} dv^{'(3)}, \tag{72}$$

which gets simplified to the expression of standard hyperbolic area

$$\int \delta\Big((v^{'(1)})^2 + (v^{'(2)})^2 - (v^{'(3)})^2 + 1\Big) dv^{'(1)} dv^{'(2)} dv^{'(3)} = \int \frac{dv^{'(1)} dv^{'(2)}}{\sqrt{(v^{'(1)})^2 + (v^{'(2)})^2 + 1}}. \tag{73}$$

The limits of the integration for the intersection region can be simplified if we look at things using the Beltrami-Klein model of hyperbolic geometry. Here, we have the Klein disc which maps the entire hyperbolic manifold onto a disk of radius one and at a unit distance height from the origin.

Now, if we define the radial distance from the origin

$$\rho^2 = (v^{'(1)})^2 + (v^{'(2)})^2, \tag{74}$$

and the radial distance of the projection on the Klein disc

$$\gamma = \frac{\rho}{\sqrt{\rho^2 + 1}}, \tag{75}$$

then in terms of these variables, Eq. (73) becomes

$$\int \frac{dv^{'(1)} dv^{'(2)}}{\sqrt{(v^{'(1)})^2 + (v^{'(2)})^2 + 1}} = \int \frac{\gamma}{\sqrt{(1-\gamma^2)^3}}\, d\gamma d\theta, \tag{76}$$

where θ is the usual angle in polar co-ordinates.

Now, the intersection region or the hyperbolic triangle has a projection which is a Euclidean triangle on the Klein disc. Therefore, the limits of integration here are straight lines in the γ and θ coordinate system. So for the

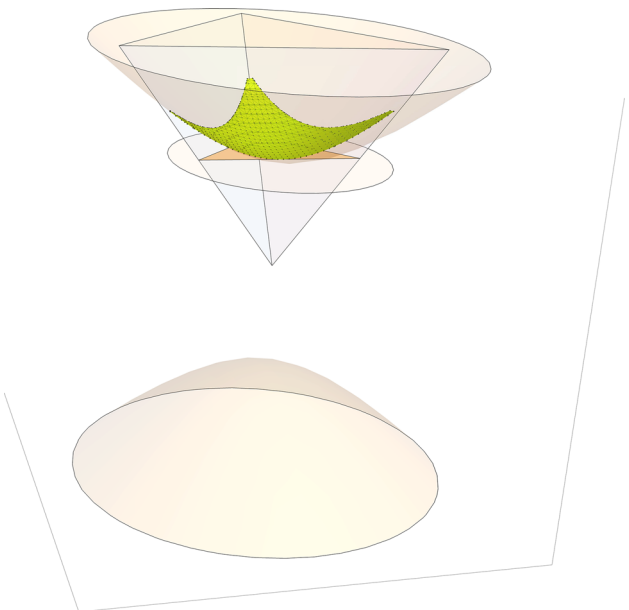

Fig. 11 Figure showing the intersection of the hyperboloid with the simplex (the green surface) and the intersection of the Klein disc and the simplex (the orange surface)

triangle diagram, we had constructed a triangle in Fig. 6, the projection on the Klein disc will also be a similar triangle with proportional side lengths.

Now, we can split that projected similar triangle into three triangles with common sides having lengths 'a', 'b', and 'c' proportional to the length of momenta p_1, p_2, and p_3, respectively. Also, the triangles subtend the angles 'θ_1', 'θ_2' and 'θ_3' on the origin.

Now, we will calculate the hyperbolic area of the triangle with side lengths 'a' and 'b' and angle 'θ_1' in between them. For this, the limits of integration for γ is between zero to the straight line connecting the tip of the triangle sides 'a' and 'b', and for θ, it is between θ_0 to $\theta_0 + \theta_1$.

$$\int_{\theta_0}^{\theta_0+\theta_1} \int_0^{\frac{ab\sin(\theta_2)}{a\sin(\theta_0-\theta_1)-b\sin(\theta_0-\theta_1-\theta_2)}} \frac{\gamma}{\sqrt{(1-\gamma^2)^3}}\, d\gamma d\theta. \tag{77}$$

This matches eq.(69) with $A[u_i] = -1$,$B[\theta] = 0$ and $C[\theta] = 1$ and it can be evaluated to the expression containing the inverse tan and inverse cot functions

$$-\tan^{-1}\left(\frac{\sqrt{1-a^2}b\sin(\theta_2)}{a-b\cos(\theta 2)}\right) - \tan^{-1}\left(\frac{a\sqrt{1-b^2}\sin(\theta_2)}{b-a\cos(\theta_2)}\right) - \cot^{-1}\left(\frac{a\sin(\theta_2)}{b-a\cos(\theta_2)}\right) - \cot^{-1}\left(\frac{b\sin(\theta_2)}{a-b\cos(\theta_2)}\right), \tag{78}$$

which gives the standard result of $\pi - \theta_2$ for the area of the 'infinite hyperbolic triangle' with two ideal vertices in the limit $a, b \to 1$.

This result can be expressed in terms of the Euclidean triangle area $absin(\theta_2)$, if we rewrite hyperbolic area integral as

$$F[k] = \int \frac{\gamma}{\sqrt{(1-k^2\gamma^2)^3}}\, d\gamma d\theta, \tag{79}$$

and expand it as a series in k^2. Therefore, we have a expression where $F[0]$ equals the Euclidean area and $F[1]$ equals the hyperbolic area. The series expansion gives

$$\begin{aligned} F[k] =& \frac{1}{k^2}\Bigg\{ -\tan^{-1}\left(\frac{a\sin(\theta_2)}{b-a\cos(\theta_2)}\right) - \tan^{-1}\left(\frac{b\sin(\theta_2)}{a-b\cos(\theta_2)}\right) - \cot^{-1}\left(\frac{a\sin(\theta_2)}{b-a\cos(\theta 2)}\right) - \cot^{-1}\left(\frac{b\sin(\theta 2)}{a-b\cos(\theta_2)}\right) \\ &+ \frac{1}{2}abk^2\sin(\theta_2) + \frac{1}{8}abk^4\sin(\theta_2)\left(a^2 + ab\cos(\theta_2) + b^2\right) \\ &+ \frac{1}{48}abk^6\sin(\theta_2)\left(3a^4 + a^2b^2\cos(2\theta_2) + 3ab\left(a^2+b^2\right)\cos(\theta_2) + 2a^2b^2 + 3b^4\right) \\ &+ \cdots (\text{terms proportional to the Euclidean area})\Bigg\}. \end{aligned} \tag{80}$$

The first four terms in the expansion add up to zero. From the fifth term onwards, we can see that the terms are proportional to the Euclidean area '$absin(\theta)$', with the fifth term being equal to the Euclidean area. This means we can express the hyperbolic area as a series of Euclidean triangles.

4.2 Bubble

For the Bubble, we can use Eq. (71) to find out the resulting expression in terms of the Euclidean area. The first term in the expansion suggests that it is proportional to the Euclidean area since $A[u_i]$ is not dependent upon θ. It is given by

$$vol_{Bubble}(\Sigma(v_i^{'\mathrm{M}})) = -\frac{iabsin(\theta 2)}{2(A[u_i])^{3/2}} + \cdots. \tag{81}$$

Now, we can see that all the terms in Eq. (71) are proportional to $i/(A[u_i])^{3/2}$. So for the stacking up of the Feynman diagrams for the scattering amplitude happens (i.e., the triangles represented by those diagrams have

common sides beginning at first order), we will multiply Eq. (71)) by $i(A[u_i])^{3/2}$, then the result will be proportional to the original result. This proportionality can be dealt with if we shift the mass for the bubble such that

$$F_{\text{Bubble}}(m_i') = i/(A[u_i])^{3/2} F_{\text{Bubble}}(m_i), \tag{82}$$

where F_{Bubble} is the expression for the Feynman integral of the Bubble diagram. Also, we only change the mass of the propagator which is unique to only one Bubble diagram in the scattering process $1 \to 2$. Hence after doing we get the first-order term equal to the Euclidean area

$$\text{vol}_{\text{Bubble}}(\Sigma(v_i^{'\text{M}})) = \frac{ab\sin(\theta 2).}{2} + \cdots \tag{83}$$

4.3 Tadpole

Now for the tadpole, we use the same method as for the bubble diagram. We shift the mass of the propagator which is unique to the tadpole diagram in the scattering process $1 \to 2$. Doing this once again, we get the first-order term equal to the Euclidean area in the expansion of the resulting expression for the tadpole diagram.

$$\text{vol}_{\text{Tadpole}}(\Sigma(v_i^{'\text{M}})) = \frac{ab\sin(\theta 2).}{2} + \cdots \tag{84}$$

5 Stacking up

Now, we see the first-order terms in the expansion of the resulting expression of the Feynman integrals has a nice geometrical viewpoint. The triangles represented by these terms have a common side as they are Euclidean areas of the resulting triangles made by the momenta and hence can be stacked up. Note that we are not following any thorough mathematical formalism for stacking up. The whole formalism is just to show that we have common sides for the triangles using this approach. A more rigorous mathematical formalism to find out a geometry is a subject of future investigation. All these triangles are shown in Figs. 6 and 7. If we just stack up the triangles in Fig. 6 using the common sides, we get the following figure, see Fig. 12.

Now, there is one more way to do the stack up, the sides where the orientation of the 'blades' of the 'whirlpool wheel' type diagram can be anticlockwise rather than the clockwise orientation here. But here, we will stick to the clockwise orientation as a convention. Now if we stack up the triangles in Fig. 7 according to the common sides approach we get, see Fig. 13. Therefore, we see that the main triangle is unaffected, but the triangles corresponding to the tadpoles and the bubbles no longer have the same area but instead stack up according to their common sides and make a quadrilateral instead of a parallelogram.

But the triangles represent only the $\text{vol}_{C^{n-1}}(\Sigma(v_i^{'\text{M}}))$ of the Feynman integral result Eq. (46), and we have a factor $\text{vol}_{\mathbb{R}^{n-1}}(\Sigma(p_i^{''\text{M}}))$ in the denominator which varies with different Feynman integrals. This factor equals the Euclidean area of the corresponding Feynman integral. Therefore, actually, it is the ratio of areas of the shapes

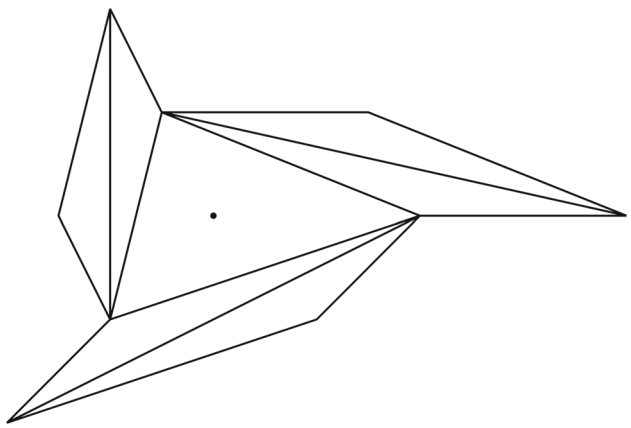

Fig. 12 Stacking up triangles—1st step

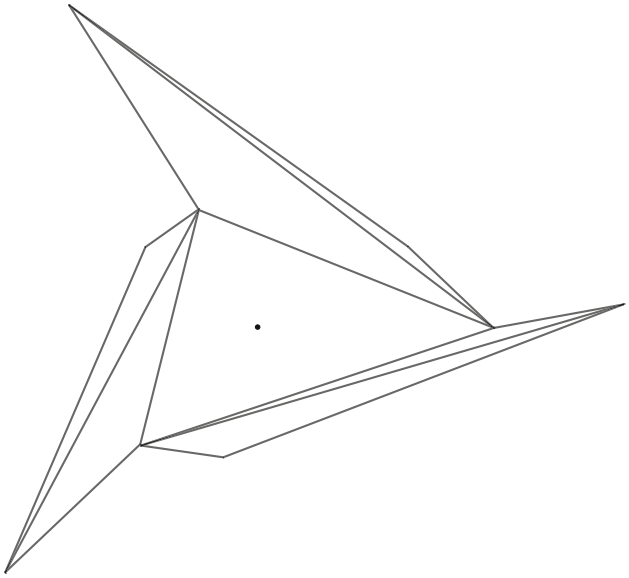

Fig. 13 Stacking up shifted triangles—1st step

which is just a mere number. In order to see something interesting, we need to keep the area of the shape in the numerator intact. For this, we need to divide and multiply all the Feynman integrals with the area of the triangle integral. We keep the dividing triangle area in the denominator as common, and now we can add up the diagrams with a scalar multiple each and all having common denominators.

$$\begin{aligned}\text{One-loop 3-point scattering amplitude} &= \sum_{I'} \int \mathrm{d}^n p \prod_{i \in I'} \frac{1}{Q_i'} \\ &= \frac{\mathrm{vol}(S^n_{1/2})}{R\,\mathrm{vol}_{\mathbb{R}^{n-1}}(\Sigma(p_i^{\mathrm{M}}))} \sum_{I'} \left(\frac{\mathrm{vol}_{\mathbb{R}^{n-1}}(\Sigma(p_i^{\mathrm{M}}))}{\mathrm{vol}_{\mathbb{R}^{n-1}}(\Sigma(p_i{}''^{\mathrm{M}}))} \right) \mathrm{vol}_{C^{n-1}}(\Sigma(v_i'^{\mathrm{M}})). \end{aligned} \tag{85}$$

Therefore, we see that the scalar multiples are the ratios of triangle areas and the areas represented by the corresponding Feynman integral. These ratios can be evaluated by first considering all the participating vectors in particular in terms of any two basis vectors out of p_1, p_2 and p_3.

5.1 Evaluation of the ratio for the bubble and tadpole diagram

We will first evaluate the ratios for the bubble diagram and the tad[pole diagrams. The area of the mapped triangle corresponding to the bubble diagram is given by

$$\text{Area of mapped triangle for the bubble} = \frac{\bar{p}_{i,\,i+1} \otimes (\bar{r}_B - \bar{p}_i)}{2}, \tag{86}$$

and for the tadpole

$$\text{Area of mapped triangle for the tadpole} = \frac{(\bar{p}_i - \bar{p}_{i+2N}) \otimes (\bar{p}_{i,\,i+1} + \bar{r}_B - \bar{p}_{i+2N})}{2}. \tag{87}$$

Here, we can see that if we choose $\bar{p}_i \| \bar{p}_{i+2N}$ then the above area formula becomes most compact expression possible. Now, if we rewrite r_B in terms of the existing two basis vectors in the area expression, i.e.,

$$\bar{r}_B = c_i^{i,\,i+1} \bar{p}_i + c_{i+1}^{i,\,i+1} \bar{p}_{i+1}, \tag{88}$$

then the area becomes

$$\text{Area of mapped triangle for the bubble} = \frac{\left(1 - c_i^{i,\,i+1} - c_{i+1}^{i,\,i+1}\right)(\bar{p}_i \otimes \bar{p}_{i+1})}{2}, \tag{89}$$

and using the parallelity convention if

$$\bar{p}_i = d_i\, \bar{p}_{i+2N}, \tag{90}$$

then

$$\text{Area of mapped triangle for the tadpole} = \frac{\left(1 + c_{i+1}^{i,\,i+1}\right)(1 - d_i)(\bar{p}_i \otimes \bar{p}_{i+1})}{2}. \tag{91}$$

We see that there is a common factor $(\bar{p}_i \otimes \bar{p}_{i+1})$ in both the area expressions. This is because of the fact that the diagonals of a parallelogram divide it into four equal half areas. For example consider the parallelogram formed by p_1, p_2, p_{12} and the origin

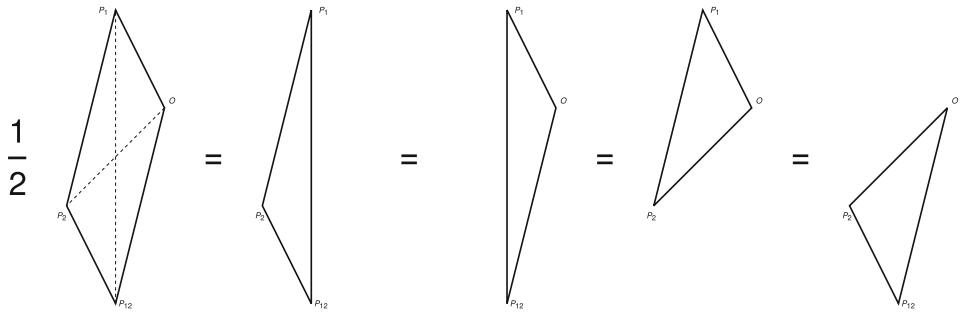

(92)

Here, the triangles p_1p_2O, Op_2p_{12}, $p_1p_2p_{12}$andOp_1p_{12} all have equal areas

Therefore, there is a common factor in the scalar multiple for the bubble and the Tadpole diagrams. For example, if we consider the area factor p_1Op_{12} coming from the tadpole then the dividing area is equal to the area of triangle p_1p_2O since they have equal areas. Hence, the scalar multiple in this case becomes

$$\frac{\text{vol}_{\mathbb{R}^{n-1}}(\Sigma(p_i^{\mathrm{M}}))}{\text{vol}_{\mathbb{R}^{n-1}}(\Sigma(p_i^{''\mathrm{M}}))} = \frac{\text{Area of}\triangle p_1p_2p_3}{\left(1 + c_{i+1}^{i,\,i+1}\right)(1 - d_i)\text{Area of}\triangle p_1p_2O}. \tag{93}$$

Now for evaluating the ratio, we need to express p_3 in terms of p_1 and p_2. Now since they are in a plane and $p_1 \neq kp_2$, we can rewrite p_3 as a linear combination of p_1 and p_2

$$p_3 = \alpha p_1 + \beta p_2, \tag{94}$$

then we can rewrite the scalar multiple as

$$
\begin{aligned}
&\frac{\text{Area of}\triangle p_1p_2p_3}{\left(1+c_{i+1}^{i,i+1}\right)(1-d_i)\text{Area of}\triangle p_1p_2O} \\
&= \frac{1}{\left(1+c_{i+1}^{i,i+1}\right)(1-d_i)}\ \frac{}{} \\
&= \frac{\text{Area of}\triangle p_1p_2O + \text{Area of}\triangle p_1Op_3 + \text{Area of}\triangle Op_2p_3}{\left(1+c_{i+1}^{i,i+1}\right)(1-d_i)\text{Area of}\triangle p_1p_2O} \\
&= \frac{p_1\otimes p_2 + p_2\otimes p_3 + p_1\otimes p_3}{\left(1+c_{i+1}^{i,i+1}\right)(1-d_i)(p_1\otimes p_2)} \\
&= \frac{\alpha+\beta+1}{\left(1+c_{i+1}^{i,i+1}\right)(1-d_i)}
\end{aligned}
\tag{95}
$$

where we have used Eq. (94) in the last step. Now α and beta β can be derived geometrically if we extend or contract p_1 and p_2 in their respective directions and try to form a triangle with p_3

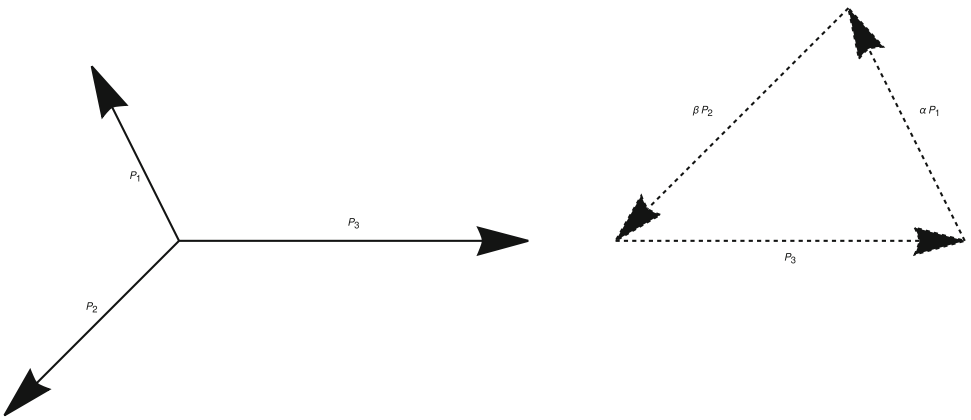

Fig. 14 p_3 as a linear combination of p_1 and p_2

Now, the sides of the triangle formed will correspond to the sides of the new parallelograms that needs to be added to the Fig. 12.

For the tadpole case, it is

$$\begin{aligned}\frac{(\alpha+\beta+1)}{\left(1+c_{i+1}^{i,i+1}\right)(1-d_i)}&\left(\text{Area for tadpole diagram}\left(\left(1+c_{i+1}^{i,i+1}\right)(1-d_i)A(\triangle p_1 O p_{12})\right)\right)\\&=(\alpha+\beta+1)((A(\triangle p_1 O p_{12})))\\&=(\alpha+\beta+1)((A(\triangle p_1 p_2 p_{12})))\\&=(A(\triangle(\alpha p_1)p_2 p_{12}))+(A(\triangle p_1(\beta p_2)p_{12}))+(A(\triangle p_1 p_2 p_{12})),\end{aligned}\tag{96}$$

and similarly for the bubble

$$\begin{aligned}&\frac{(\alpha+\beta+1)}{\left(1-c_i^{i,i+1}-c_{i+1}^{i,i+1}\right)}\left(\text{Area for bubble diagram}\left(\left(1-c_i^{i,i+1}-c_{i+1}^{i,i+1}\right)A(\triangle p_1 p_2 p_{12})\right)\right)\\&=(A(\triangle(\alpha p_1)p_2 p_{12}))+(A(\triangle p_1(\beta p_2)p_{12}))+(A(\triangle p_1 p_2 p_{12})).\end{aligned}\tag{97}$$

Summing both of them gives

$$\begin{aligned}&(\alpha+\beta+1)((A(\triangle p_1 p_2 p_{12}))+(A(\triangle p_1 O p_{12})))\\&\quad=(\alpha+\beta+1)(\text{Area for quadrilateral}(A(\square p_1 p_2 O p_{12})))\\&\quad=((A(\square(\alpha p_1)\otimes p_{12})))+(A(\square(\beta p_2)\otimes p_{12}))+(A(\square p_1 p_2 O p_{12})).\end{aligned}\tag{98}$$

Diagrammatically:

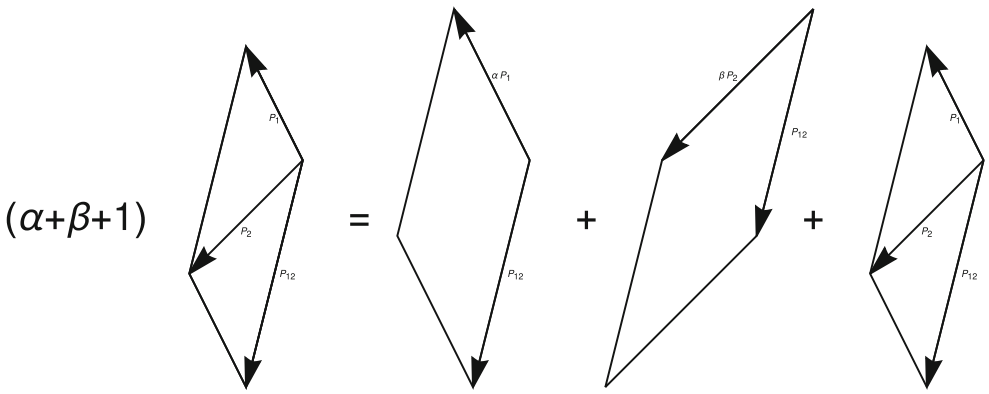

(99)

Therefore, finally doing this for all the seven diagrams, we finally get a figure, see Fig. 15

Note that this is not a unique way representing the whole scattering amplitude. A more rigorous approach towards finding the precise geometry is a subject of future investigation.

6 Discussion and conclusions

Nima Arkani Hamed and co-workers were inspired by $N = 4$ SYM were able to observe that positive geometries make a natural appearance in the study of the trees and the integrands of these theories. Having started, they were able to consider such constructions for scattering amplitudes for bi-adjoint ϕ^3 theory also at the tree-level. This gave rise to the amplituhedron (associahedron) for this theory. This was then extended to the construction of a halohedron wherein the integrands at one-loop were constructed. These, in turn, lead to cluster polytopes as constructed by Nima. The natural question then arises as to whether the one-loop integrals themselves will permit any kind of polytope construction. In the present work, we give an explicit construction of such a polytope construction based on the one-loop Feynman integral computation and methods introduced by Schnetz following the seminal work of Davydychev and Delbourgo [24]. In contrast to the work of associahedron and halohedron, the present work relies not on positive geometries but hyperbolic geometries. This feature was already observed by

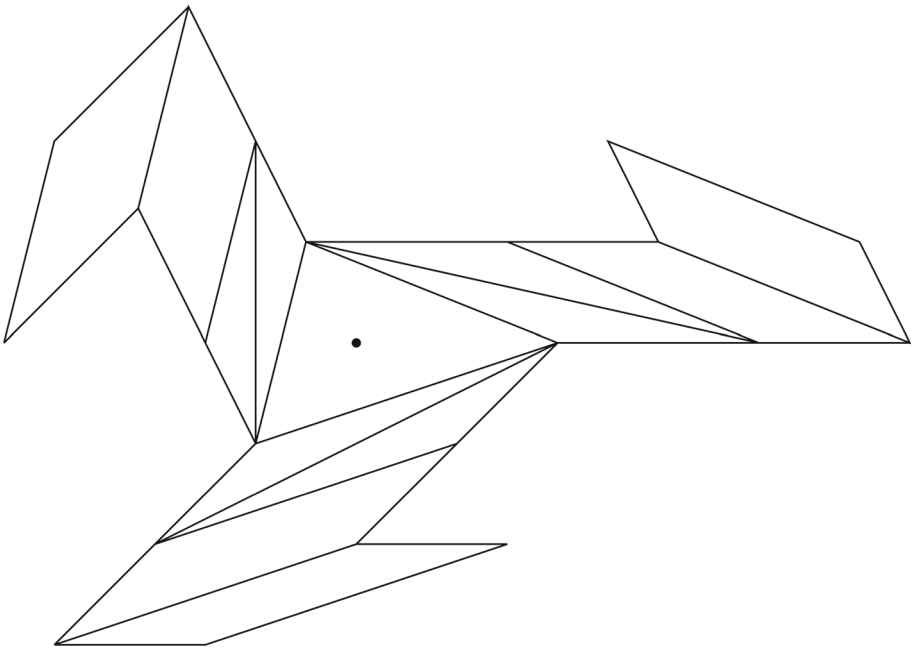

Fig. 15 Final figure

Schnetz. The hyperbolic geometry rests on Eqs. (57) and (63) of [23]. The independent variables and the constraints on them in the Feynman representation naturally led to their interpretations as lying in hyperbolic geometry. Note that the original construction does not suffice to accommodate the extension to scattering amplitudes. In order to achieve this end, we have had to introduce a new grammar, wherein a distinction has to be made between internal propagators carrying loop momenta and those that do not. In this extended system, the hyperbolic geometry becomes apparent in Eq. (39). It may be noted that there are considerable algebraic simplifications that allow this to occur. That done, it is not yet obvious that the resulting triangles would actually produce a polytope. In the example at hand, this is found to be the case by explicit construction. Our work is motivated by the ideas using which the amplituhedron and halohedrons, and cluster polytopes are constructed. Primarily we rely on the principle of common sides of polytopes observed in Fig. 16 of [15]. Also, we restrict the analysis to first order series expansion of the one-loop amplitude.

This is an introductory level work to find out a hidden geometry of scattering amplitudes at the integral level and hence yet to attain a thorough mathematical rigor and perfection. We believe that the work in Sects. 4 and 5 can be formulated in a more concrete mathematical framework and is a subject of future investigation. The key achievements of our work include raising internal and loop propagators to a level where the distinction is only in terms of specific indices, Eqs. (21), (27), and (33), finding a single equation which relates the masses of both internal and the loop propagators to radii of spheres, Eq. (30), encoding the information about all the masses and the momenta and thus the information about all the parameters of the scattering amplitude in a single 2D geometrical picture which is a very fundamental and exciting way of looking at it. And finding out a general quadric surface equation, Eq. (39), which unifies the hyperbolic geometries of the triangle, bubble, and tadpole in a single equation which is a solid proof towards a more concrete mathematical framework for the unification. It is, of course, natural to ask whether this can be extended to even higher orders in series expansion, loops, and other theories and subsequently becomes a work for the future.

Also, an important motivation for this work is related to the fact that the scattering amplitude is a physical observable, which is fundamentally different than the theoretical lagrangian of a quantum field theory. Therefore, this study is motivated towards finding out a geometry of the scattering amplitude itself rather than focusing on the lagrangian. The scattering amplitude, in many terms, is actually more fundamental than the lagrangian. This is supported by the studies conducted on the S-matrix bootstrap program and the recent work on positive geometries by Nima Arkani Hamed. Also, an enormous calculational simplification happens when we move from Feynman diagrams towards scattering amplitudes evident in the gluon-scattering amplitudes at the tree level giving us a hint towards the fact the scattering amplitudes are more fundamental. Our approach towards finding out a geometry at the integral level will help us go beyond the clutches of perturbation theory as we can add up the integrals at different loop orders in perturbation theory. This is a significant advancement from the positive geometry at the integrand level, as different loop orders there cannot be directly summed up. Hence, our work is an important step towards discovering the geometry of scattering amplitudes up to all orders. The geometrical picture definitely hints

towards finding out the scattering amplitude exactly, independent of the perturbation theory approach, as all the parameters/arguments in the scattering amplitude can be put on geometrically as we have done in our work. The S-matrix bootstrap program definitely hints towards the existence of a scattering amplitude independent of the perturbation theory and hence is in favor of our claim.

Acknowledgements AD thanks Prof. B. Ananthanarayan and Prof. Daniel Wyler for adding valuable discussions and comments during the course of this work. AD also thanks MHRD, India, for providing the required funding during the course of this work.

Funding This research was supported by Indian Institute of Science.

Data availability statement Data sharing is not applicable to this article as no datasets were generated or analysed during the current study.

Declarations

Conflict of interest We have no conflicts of interest to disclose.

Appendix

See Table 1.

Derivation of Eq. (30)

In [23], we saw that the constant r is defined using the equation

$$(p_i - c)^2 + m_i^2 = r^2, \quad i = 1, \ldots, n+1. \tag{100}$$

This equation is valid since the choice of vectors p_i is arbitrary such that p_{ij} is fixed. Also there always exists a solution to r, for e.g. for the $N = 3$ case, there always exists a point c on the p plane which is equidistant from the tip of the vectors m_i Fig. 16.

Since p_i is arbitrary we can choose point c to be the origin in our case. So Eq. (100) takes the form

$$p_i^2 + m_i^2 = r^2, \quad i = 1, \ldots, n+1. \tag{101}$$

So in the case where $a_i = 1$ the above equation is valid as the arbitrariness of the p_i is only vaild here. For the other cases, i.e., $a_i = 0$, the $p_i' = p_{i-N,\, i-N+1}$ being the external momenta are fixed. Also for case where $p_i' = 0$ its a constant and hence devoid of any arbitrariness. For those cases we may write out the similar equation

$$p_i^{'2} + m_i^{'2} = r_i^2, \quad i = 1, \ldots, n+1. \tag{102}$$

Table 1 Table showing the involved $Q_i's$ and $p_i's$ for a particular Feynman diagram

Diagrams		Q_i' involved	Momenta involved in v_i'	
Type	Identity		p_i' (Without shift)	p_i'' (With shift)
Tadpole	T2	Q_2', Q_5', Q_8'	$p_2, p_{23}, 0$	$p_2, p_{23} - r_B, p_8$
	T4	Q_3', Q_6', Q_9'	$p_3, p_{31}, 0$	$p_3, p_{31} - r_B, p_9$
	T6	Q_1', Q_4', Q_7'	$p_1, p_{12}, 0$	$p_1, p_{12} - r_B, p_7$
Bubble	T3	Q_2', Q_3', Q_5'	p_2, p_{23}, p_3	$p_2, p_{23} - r_B, p_3$
	T5	Q_1', Q_3', Q_6'	p_3, p_{31}, p_1	$p_3, p_{31} - r_B, p_1$
	T7	Q_1', Q_2', Q_4'	p_2, p_{12}, p_1	$p_2, p_{12} - r_B, p_1$
Triangle	T1	Q_1', Q_2', Q_3'	p_2, p_3, p_1	p_2, p_3, p_1

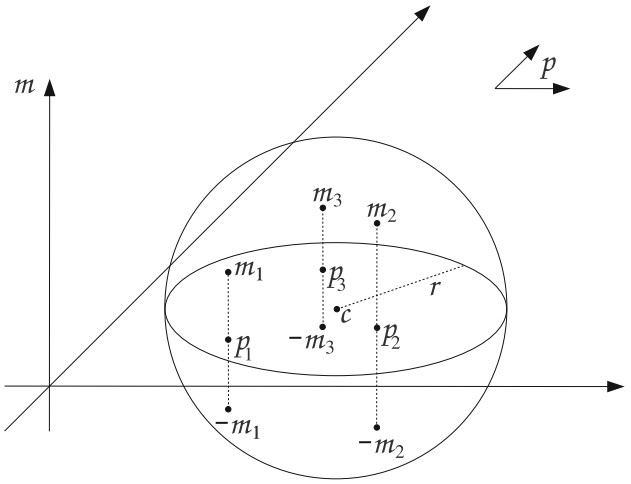

Fig. 16 The sphere spanned by the momenta and masses

Here we see that f4 or each internal propagator there is a corresponding constant r_i and hence all the conditions of the value of internal propagators being fixed are satisfied.

Now looking at the form of Eq. (27), we see that p_i^2 and m_i^2 are being multiplied by the constant coefficients a_j. So we need to multiply a_j to Eq. (102)

$$a_j^2(m_i^{'2} + p_i^{'2}) = a_j^2 r_i^{'2}. \tag{103}$$

Also there are terms with the i and j indices switched and hence we also need the following equation:

$$a_i^2(m_j^{'2} + p_j^{'2}) = a_i^2 r_j^{'2}. \tag{104}$$

Finally summing the two equations, we conclude that the general equation identical to Eq. (100) in our case which will replace the $m_i's$ in Eq. (27) will be of the form

$$a_i^2(m_j^{'2} + p_j^{'2}) + a_j^2(m_i^{'2} + p_i^{'2}) = a_i^2 r_j^2 + a_j^2 r_i^{'2}. \tag{105}$$

This equation acts on Eq. (27) in a similar way like Eq. (100) acts on Eq. (57) of [23]. But there is a limitation in Eq. (105), if we substitute it in Eq. (27) we get a dot product of the form:

$$\begin{aligned} &\frac{(a_j p_i' - a_i p_j')^2 + a_j^2 m_i^{'2} + a_i^2 m_j^{'2}}{2}, \\ &= \left[a_j p_i' - i\left(\sqrt{\frac{a_j r_i^2 + a_i r_j^2}{2}}\right)\right] \cdot \left[a_i p_j' - i\left(\sqrt{\frac{a_j r_i^2 + a_i r_j^2}{2}}\right)\right]. \end{aligned} \tag{106}$$

We can see that inside the term analogous to the dot product of Eq. (60) in [23], $\left(\sqrt{\frac{a_j r_i^2 + a_i r_j^2}{2}}\right)$ is not a constant in contrast to r there as both a_i and r_i change for different i and j. Hence this can't be a valid extension of the theory presented in [23].

This issue can be resolved if instead of r_i in the RHS of Eq. (102) which varies with i, we have a constant say r_{BT}. This is possible if we try to make a similar geometrical arrangement like Fig. 16 which lead to Eq. (101) where the RHS is a constant. For this we once again make a triangle but now with position vectors for the vertices given by $p_{i-N,\,i-N+1}$ instead of p_i, see Fig. 17.

Also the corresponding m_i vectors are at the vertices perpendicular to the plane of the external momenta once again making a sphere. But this time the center of the sphere is different from the origin of the position vectors of the vertices. If we denote this shift by a vector $\bar{r}_B$, see Fig.(18) then Eq. (102) gets modified to

$$(\bar{p}_i' - \bar{r}_B)^2 + m_i^{'2} = r_{BT}^2, \quad i = 1, \ldots, n+1. \tag{107}$$

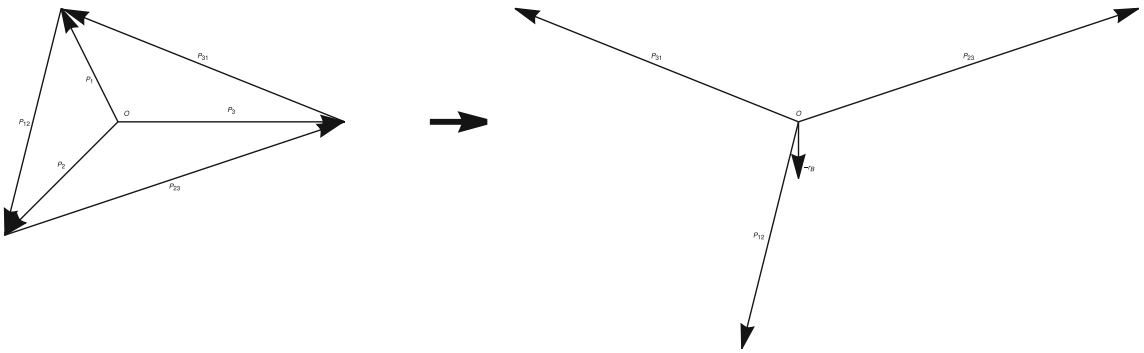

Fig. 17 The transformed triangle

The RHS of this equation is a constant and hence it meets the requirements of having a constant imaginary part in the terms of the dot product in Eq. (106). But this comes at the cost of having a shift $\bar{r}_B$ for the bubble case.

For the tadpole case, we can rewrite a similar equation with the RHS same as Eq. (107)

$$p_i^{''2} + m_i^{'2} = r_{BT}^2, \quad i = 1, \ldots, n+1. \tag{108}$$

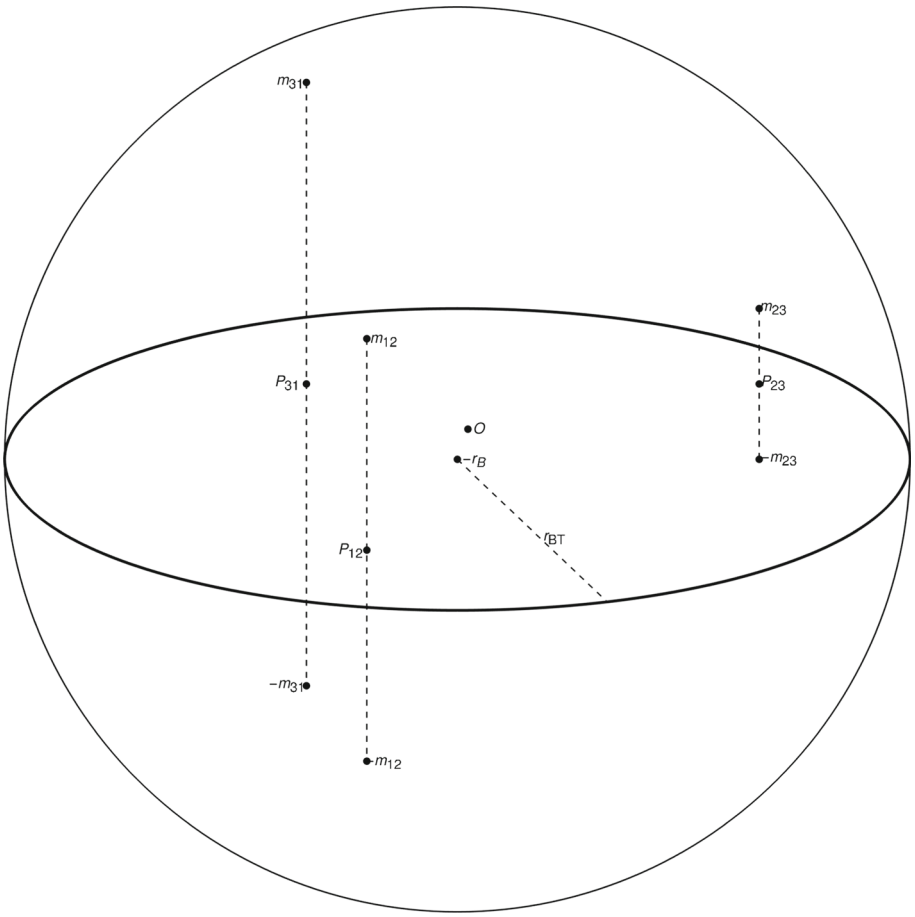

Fig. 18 The transformed sphere

Here the value of p_i'' is decided by the initial condition of the value of masses m_i and the constant r_{BT}. So if we define p_i'' as

$$p_i^{''2} = \begin{cases} p_i^2, & i = 1, \ldots, N \\ (p_{i-N,\, i-N+1} - r_B)^2, & i = N+1, \ldots, 2N \\ r_{BT}^2 - m_i^{'2} & i = 2N+1, \ldots, 3N \end{cases}, \tag{109}$$

then for the $a_i = 0$ case we can rewrite Eq. (105) as

$$a_i^2(m_j^{'2} + p_j^{''2}) + a_j^2(m_i^{'2} + p_i^{''2}) = (a_i^2 + a_j^2) r_{BT}^2. \tag{110}$$

To include the $a_i = 1$ case, finally we will add a term $2a_i a_j r^2$ to the RHS of the above equation:

$$a_i^2(m_j^{'2} + p_j^{''2}) + a_j^2(m_i^{'2} + p_i^{''2}) = (a_i^2 + a_j^2) r_{BT}^2 + 2a_i a_j r^2. \tag{111}$$

So instead of Eq. (106) we have

$$\begin{aligned} &\frac{(a_j p_i'' - a_i p_j'')^2 + a_j^2 m_i^{'2} + a_i^2 m_j^{'2}}{2} \\ &= \left[a_j p_i' - i a_j \left(\sqrt{r^2 + r_{BT}^2}\right)\right] \cdot \left[a_i p_j' - i a_i \left(\sqrt{r^2 + r_{BT}^2}\right)\right] + (a_i - a_j)^2 r_{BT}^2. \end{aligned} \tag{112}$$

Now apart form the constants a_i, a_j and an additional shift term, the RHS is exactly analogous to the dot product in [23]. So this is the proper extension of the theory there.

Significance of constant r and the term $2a_i a_j r^2$

Now we will try to understand the significance of the constant r and the term $2a_i a_j r^2$. If we put a_i and a_j equal to one in Eq. (111), we get:

$$(m_j^{'2} + p_j^{''2}) + (m_i^{'2} + p_i^{''2}) = 2r_{BT}^2 + 2r^2. \tag{113}$$

This can be thought of as being equivalent to:

$$m_i^{'2} + p_i^{''2} = r_{BT}^2 + r^2. \tag{114}$$

Since this is valid only when all $a_i's = 1$, this equation is equivalent to Eq. (101) and hence r_{BT} and r ought to be a constant for different values of i. Also for a_i or $a_j = 0$, Eq. (111) becomes equal to Eq. (107) and Eq. (108). This shows that Eq. (111) covers all the cases originating from different values of a_i perfectly.

Note that the term $2a_i a_j r^2$ in Eq. (111) satisfies different conditions originating from different values of a_i, the need to write the expression in Eq. (27) in form of a dot product and the need to have a constant r inside the complex part of the participating terms within the dot product all simultaneously. Also this term cannot be derived like the other terms in the RHS of Eq. (111). It is more of like a conjecture which satisfies all the required conditions. Hence we can say that Eq. (111) exists at a more fundamental level than Eq. (100), satisfying the more general mathematical formalism which includes the loop and internal propagators under a single framework.

Emergence of an additional dimension in the complex plane using Eq. (111)

Looking at the form of Eq. (112), we see that the constants r and r_{BT} appear to be perpendicular to each other within the complex plane. So Eq. (111) which is a conjecture by itself hints at the emergence of an additional dimension within the complex plane. The equation which was designed to encapsulate all the possibilities arising out of the different values of a_i actually paved the way to the idea of an additional dimension.

Proofs of Eqs. (58) and (59)

Now the contents of the first line of the diagonalizable matrix A in Eq. (52) can be rewritten in a concise way as

$$A_{ij} = \alpha_k^{'(i)} a_k a_m \alpha_j^{'(m)} \left(p_k^{'(l)} \hat{l}\right) \cdot \left(p_j^{'(l)} \hat{l}\right). \tag{115}$$

Similar reasoning can be given for the second line. We will discuss about it in detail later. Here $p_k^{'(l)}$ represents the lth component of the vector $p'_k - iR$. After the dot product evaluation this becomes

$$A_{ij} = \alpha_k^{'(i)} a_k a_m \alpha_j^{'(m)} p'_{kj}, \tag{116}$$

where p'_{kj} is the dot product of two vectors p'_k and p'_j. Now the eigenvalue equation can be obtained by taking the determinant of this matrix subtracted by eigenvalue times the identity matrix and then equating it to zero.

$$\mathrm{Det}[A - \lambda I] = 0. \tag{117}$$

The resulting matrix whose determinant is zero can be written in a concise way as

$$A'_{ij} = \alpha_k^{'(i)} a_k a_m \alpha_j^{'(m)} p'_{kj} - \lambda \delta_{ij}. \tag{118}$$

Also the determinant of this matrix can be written in terms of the Levi-Civita tensors [31] as

$$\mathrm{Det}\left[A'_{ij}\right] = \frac{1}{n!} \varepsilon_{i_1 \cdots i_n} \varepsilon_{j_1 \cdots j_n} A'_{i_1 j_1} \cdots A'_{i_n j_n}. \tag{119}$$

And hence the eigenvalue equation becomes

$$\varepsilon_{i_1 \cdots i_n} \varepsilon_{j_1 \cdots j_n} \left(\alpha_{k_1}^{'(i_1)} a_{k_1} a_{m_1} \alpha_{j_1}^{'(m_1)} p'_{k_1 j_1} - \lambda \delta_{i_1 j_1}\right) \cdots \left(\alpha_{k_n}^{'(i_n)} a_{k_n} a_{m_n} \alpha_{j_n}^{'(m_n)} p'_{k_n j_n} - \lambda \delta_{i_n j_n}\right) = 0. \tag{120}$$

where summation over repeated indices is implied. Now if we consider a set

$$I' = \{1', 2', ..., (n-s)'\} \subseteq I = \{1, 2, ..., n\}, \tag{121}$$

for $s \leq n$ and $s \in \mathbb{N}$, then the eigenvalue equation can be written as a polynomial equation in λ:

$$\sum_{s=0}^{n} \lambda^s a_{k_{1'}} a_{m_{1'}} \cdots a_{k_{(n-s)'}} a_{m_{(n-s)'}} \times \left(\alpha_{k_{1'}}^{'(i_{1'})} \alpha_{j_{1'}}^{'(m_{1'})} \cdots \alpha_{k_{(n-s)'}}^{'(i_{(n-s)'})} \alpha_{j_{(n-s)'}}^{'(m_{(n-s)'})} p'_{k_{1'} j_{1'}} \right.$$
$$\left. \cdots p'_{k_{(n-s)'} j_{(n-s)'}} \varepsilon_{i_1 \cdots i_n} \varepsilon_{j_1 \cdots j_n}\right) = 0. \tag{122}$$

Here the bracket indicates that the summation within the bracket is considered at first. In order to prove Eq. (58), we need to show that the term with $s = 0$ is zero when one of the $a'_i s = 0$. For this we need to show that for the $s = 0$ case, only the term with full multiplicity of $a'_i s$ is non-zero and all the other terms with less multiplicity cancel.

Case s=0

First of all we will consider the term with least multiplicity of $a'_i s$, i.e., the term with all the $a'_i s$ equal. This is possible only when all the 'a-indices' in eq.(122) are equal:

$$k_{1'} = m_{1'} = k_{2'} = m_{2'} = \cdots k_{(n-s)'} = m_{(n-s)'} = \omega \qquad \text{...least multiplicity,} \tag{123}$$

where ω is a constant and $1 \leq \omega \leq n$ and the corresponding a, we denote by a constant a_ω. So the $s = 0$ term in Eq. (122) takes the form:

$$a_\omega^{2n} \left(\alpha_\omega^{'(i_1)} \alpha_{j_1}^{'(\omega)} \alpha_\omega^{'(i_2)} \alpha_{j_2}^{'(\omega)} \cdots \alpha_\omega^{'(i_n)} \alpha_{j_n}^{'(\omega)} p'_{\omega j_1} \cdots p'_{\omega j_n} \varepsilon_{i_1 \cdots i_n} \varepsilon_{j_1 \cdots j_n}\right). \tag{124}$$

Note that for this case since we have $s = 0$, the set $I' = I$ and hence we have removed the dash from all the numbers. We need to prove that the terms of this form cancel each so that the least multiplicity contribution is zero. This can be checked by using the property that the Levi-Civita tensors change their sign when we swap two of their indices. So if we swap i_j by i_k, we can see that the expression in Eq. (124) remains the same but the sign changes

$$\begin{aligned} & a_\omega^{2n}\Big(\alpha_\omega^{'(i_1)}\alpha_{j_1}^{'(\omega)}\cdots\alpha_\omega^{'(i_j)}\cdots\alpha_\omega^{'(i_k)}\cdots\alpha_\omega^{'(i_n)}\alpha_{j_n}^{'(\omega)}p'_{\omega j_1}\cdots p'_{\omega j_n}\varepsilon_{i_1\cdots i_j\cdots i_k\cdots i_n}\varepsilon_{j_1\cdots j_n}\Big) \\ & \quad = -a_\omega^{2n}\Big(\alpha_\omega^{'(i_1)}\alpha_{j_1}^{'(\omega)}\cdots\alpha_\omega^{'(i_k)}\cdots\alpha_\omega^{'(i_j)}\cdots\alpha_\omega^{'(i_n)}\alpha_{j_n}^{'(\omega)}p'_{\omega j_1}\cdots p'_{\omega j_n}\varepsilon_{i_1\cdots i_k\cdots i_j\cdots i_n}\varepsilon_{j_1\cdots j_n}\Big), \end{aligned} \tag{125}$$

and hence there is a counter-term which cancels every term in all possible permutations of the set $i_1\cdots i_n$ within $\varepsilon_{i_1\cdots i_n}$. This is also true if we swap j_k and j_l from $\varepsilon_{j_1\cdots j_n}$. The corresponding terms cancel each other and hence we a zero contribution from the least multiplicity term.

Now we will consider the case where one of the indices is unequal:

$$k_{1'} = m_{1'} = k_{2'} = m_{2'} = \cdots k_{(n-s)'} = \omega \neq m_{(n-s)'} = \rho \quad \text{...second least multiplicity.} \tag{126}$$

For this case, the replacement of i_j and i_k brings the same result as the previous case for any j and k, but the replacement of j_k and j_l produces two different terms for $j/l = (n-s)'$. These different terms can be framed to resemble a single form and then cancelled only if we choose two different sets of second least multiplicity:

$$k_{1'} = m_{1'} = k_{2'} = m_{2'} = \cdots k_{(n-s)'} = \omega \neq m_k = \rho, \tag{127}$$

and

$$k_{1'} = m_{1'} = k_{2'} = m_{2'} = \cdots k_{(n-s)'} = \omega \neq m_l = \rho. \tag{128}$$

Then the corresponding terms cancel each other upon swapping of j_k and j_l:

$$\begin{aligned} & a_\omega^{2n-1}a_\rho\Big(\alpha_\omega^{'(i_1)}\alpha_{j_1}^{'(\omega)}\cdots\alpha_{j_k}^{'(\rho)}\cdots\alpha_{j_l}^{'(\omega)}\cdots\alpha_\omega^{'(i_n)}\alpha_{j_n}^{'(\omega)}p'_{\omega j_1}\cdots p'_{\omega j_n}\varepsilon_{i_1\cdots i_n}\varepsilon_{j_1\cdots j_k\cdots j_l\cdots j_n}\Big). \\ & \quad = -a_\omega^{2n-1}a_\rho\Big(\alpha_\omega^{'(i_1)}\alpha_{j_1}^{'(\omega)}\cdots\alpha_{j_l}^{'(\omega)}\cdots\alpha_{j_k}^{'(\rho)}\cdots\alpha_\omega^{'(i_n)}\alpha_{j_n}^{'(\omega)}p'_{\omega j_1}\cdots p'_{\omega j_n}\varepsilon_{i_1\cdots i_n}\varepsilon_{j_1\cdots j_l\cdots j_k\cdots j_n}\Big) \end{aligned} \tag{129}$$

So in this way we can cancel the second least multiplicity terms and using the similar method we can cancel the terms with higher multiplicity.

For the term term with maximum multiplicity, only specific permutations do not cancel. All other permutations can be cancelled using the above method. The permutation which does not cancel has the form for the indices:

$$k_{1'} = m_{1'} = \omega_1 \neq k_{2'} = m_{2'} = \omega_2 \neq \cdots \neq k_{(n-s)'} = m_{(n-s)'} = \omega_{(n-s)} \text{ ...max multiplicity.} \tag{130}$$

The corresponding term in Eq. (122) takes the form

$$a_{\omega_1}^2 a_{\omega_2}^2\cdots a_{\omega_n}^2\Big(\alpha_{\omega_1}^{'(i_1)}\alpha_{j_1}^{'(\omega_1)}\alpha_{\omega_2}^{'(i_2)}\alpha_{j_2}^{'(\omega_2)}\cdots\alpha_{\omega_n}^{'(i_n)}\alpha_{j_n}^{'(\omega_n)}p'_{\omega_1 j_1}\cdots p'_{\omega_n j_n}\varepsilon_{i_1\cdots i_n}\varepsilon_{j_1\cdots j_n}\Big). \tag{131}$$

Now if we replace i_k by i_l, then in order to get the same form first we need to replace ω_k by ω_l and then j_k by j_l as a second replacement. After this we not only get the same form but also with the same sign:

$$\begin{aligned} & a_{\omega_1}^2\cdots a_{\omega_n}^2\Big(\alpha_{\omega_1}^{'(i_1)}\alpha_{j_1}^{'(\omega_1)}\cdots\alpha_{\omega_k}^{'(i_k)}\alpha_{j_k}^{'(\omega_k)}\cdots\alpha_{\omega_l}^{'(i_l)}\alpha_{j_l}^{'(\omega_l)} \\ & \qquad \cdots\alpha_{\omega_n}^{'(i_n)}\alpha_{j_n}^{'(\omega_n)}p'_{\omega_1 j_1}\cdots p'_{\omega_n j_n}\varepsilon_{i_1\cdots i_k\cdots i_l\cdots i_n}\varepsilon_{j_1\cdots j_k\cdots j_l\cdots j_n}\Big) \\ & = a_{\omega_1}^2\cdots a_{\omega_n}^2\Big(\alpha_{\omega_1}^{'(i_1)}\alpha_{j_1}^{'(\omega_1)}\cdots\alpha_{\omega_l}^{'(i_l)}\alpha_{j_l}^{'(\omega_l)}\cdots\alpha_{\omega_k}^{'(i_k)}\alpha_{j_k}^{'(\omega_k)} \\ & \qquad \cdots\alpha_{\omega_n}^{'(i_n)}\alpha_{j_n}^{'(\omega_n)}p'_{\omega_1 j_1}\cdots p'_{\omega_n j_n}\varepsilon_{i_1\cdots i_l\cdots i_k\cdots i_n}\varepsilon_{j_1\cdots j_l\cdots j_k\cdots j_n}\Big). \end{aligned} \tag{132}$$

So this means that the terms of this form don't cancel and are the only species which contribute to the $s = 0$ term. These are the maximum multiplicity terms and hence if any of the $a_i's$ is zero, this term will consequently

vanish. This will lead to eq.(122) to be of the form:

$$\sum_{s=1}^{n}\lambda^{s}a_{k_{1'}}a_{m_{1'}}\cdots a_{k_{(n-s)'}}a_{m_{(n-s)'}}\Big(\alpha^{'(i_{1'})}_{k_{1'}}\alpha^{'(m_{1'})}_{j_{1'}}\cdots\alpha^{'(i_{(n-s)'})}_{k_{(n-s)'}}\alpha^{'(m_{(n-s)'})}_{j_{(n-s)'}}p'_{k_{1'}j_{1'}}$$
$$\cdots p'_{k_{(n-s)'}j_{(n-s)'}}\varepsilon_{i_1\cdots i_n}\varepsilon_{j_1\cdots j_n}\Big)=0. \tag{133}$$

So we can take out a λ term common and hence one of the solutions of this equation will always be a trivial solution. This proves Eq. (58). Similar reasoning goes for the second line terms in Eq. (52). They also give rise to hyperboloid with one flat axis and hyperboloid with two flat axis and hence consequently producing hyperboloid with one flat axis as the final result. We need to dig deeper to higher values of s in order to generalize the proof. The next proof for Eq. (59) will require the $s=1$ term.

Case s=1

Here we will first consider the term with maximum multiplicity.

$$k_{1'}=m_{1'}=\omega_{1'}\neq k_{2'}=m_{2'}=\omega_{2'}\neq\cdots\neq k_{(n-s)'}=\omega_{(n-s)'}\neq m_{(n-s)'}=\omega_{(n-s+1)'}\ \text{...max multiplicity.} \tag{134}$$

Note that we have retained the dash in the indices of omega as I' is a proper subset of I for this case. The corresponding term in Eq. (122) is given by:

$$a^2_{\omega_{1'}}a^2_{\omega_{2'}}\cdots a^2_{\omega_{(n-2)'}}a_{\omega_{(n-1)'}}a_{\omega_{n'}}\lambda\Big(\alpha^{'(i_{1'})}_{\omega_{1'}}\alpha^{'(\omega_{1'})}_{j_{1'}}\alpha^{'(i_{2'})}_{\omega_{2'}}\alpha^{'(\omega_{2'})}_{j_{2'}}\cdots\alpha^{'(i_{(n-2)'})}_{\omega_{(n-2)'}}\alpha^{'(\omega_{(n-2)'})}_{j_{(n-2)'}}\alpha^{'(i_{n'})}_{\omega_{(n-1)'}}$$
$$\alpha^{'(\omega_{n'})}_{j_{n'}}p'_{\omega_{1'}j_{1'}}\cdots p'_{\omega_{(n-1)'}j_{(n-1)'}}\varepsilon_{i_1\cdots i_n}\varepsilon_{j_1\cdots j_n}\Big). \tag{135}$$

Here also we can use the method in the previous case for the maximum multiplicity. We swap $i_{k'}$ by $i_{l'}$, then consecutively swapping $\omega_{k'}$ by $\omega_{l'}$ and $j_{k'}$ by $j_{l'}$, we get the same form and again with the same sign.

$$\begin{aligned}&a^2_{\omega_{1'}}a^2_{\omega_{2'}}\cdots a^2_{\omega_{k'}}\cdots a^2_{\omega_{l'}}\cdots a^2_{\omega_{(n-2)'}}a_{\omega_{(n-1)'}}a_{\omega_{n'}}\lambda\\&\quad\times\Big(\alpha^{'(i_{1'})}_{\omega_{1'}}\alpha^{'(\omega_{1'})}_{j_{1'}}\cdots\alpha^{'(i_{k'})}_{\omega_{k'}}\cdots\alpha^{'(i_{l'})}_{\omega_{l'}}\cdots\alpha^{'(i_{n'})}_{\omega_{(n-1)'}}\alpha^{'(\omega_{n'})}_{j_{n'}}p'_{\omega_{1'}j_{1'}}\\&\quad\cdots p'_{\omega_{(n-1)'}j_{(n-1)'}}\varepsilon_{i_1\cdots i_k\cdots i_l\cdots i_n}\varepsilon_{j_1\cdots j_k\cdots j_l\cdots j_n}\Big)\\&=a^2_{\omega_{1'}}a^2_{\omega_{2'}}\cdots a^2_{\omega_{l'}}\cdots a^2_{\omega_{k'}}\cdots a^2_{\omega_{(n-2)'}}a_{\omega_{(n-1)'}}a_{\omega_{n'}}\lambda\\&\times\Big(\alpha^{'(i_{1'})}_{\omega_{1'}}\alpha^{'(\omega_{1'})}_{j_{1'}}\cdots\alpha^{'(i_{l'})}_{\omega_{l'}}\cdots\alpha^{'(i_{k'})}_{\omega_{k'}}\cdots\alpha^{'(i_{n'})}_{\omega_{(n-1)'}}\alpha^{'(\omega_{n'})}_{j_{n'}}p'_{\omega_{1'}j_{1'}}\\&\quad\cdots p'_{\omega_{(n-1)'}j_{(n-1)'}}\varepsilon_{i_1\cdots i_l\cdots i_k\cdots i_n}\varepsilon_{j_1\cdots j_l\cdots j_k\cdots j_n}\Big).\end{aligned} \tag{136}$$

Hence this term has a non-zero contribution to the $s=1$ term in Eq. (122). Now we will consider the next to maximum multiplicity or second maximum multiplicity term. The indices for this case are given by

$$k_{1'}=m_{1'}=\omega_{1'}\neq k_{2'}=m_{2'}=\omega_{2'}\neq\cdots\neq k_{(n-s)'}=m_{(n-s)'}=\omega_{(n-s)'}\ \text{... next to max multiplicity,} \tag{137}$$

and the corresponding term is given by

$$a^2_{\omega_{1'}}a^2_{\omega_{2'}}\cdots a^2_{\omega_{(n-2)'}}a^2_{\omega_{(n-1)'}}\lambda\Big(\alpha^{'(i_{1'})}_{\omega_{1'}}\alpha^{'(\omega_{1'})}_{j_{1'}}\alpha^{'(i_{2'})}_{\omega_{2'}}\alpha^{'(\omega_{2'})}_{j_{2'}}\cdots\alpha^{'(i_{(n-1)'})}_{\omega_{(n-1)'}}\alpha^{'(\omega_{(n-1)'})}_{j_{(n-1)'}}p'_{\omega_{1'}j_{1'}}$$
$$\cdots p'_{\omega_{(n-1)'}j_{(n-1)'}}\varepsilon_{i_1\cdots i_n}\varepsilon_{j_1\cdots j_n}\Big). \tag{138}$$

Here also we can apply the previous method for maximum multiplicity and conclude that the contribution of this second maximum multiplicity term is non-zero for the $s=1$ term in Eq. (122). Now consequently we will move on to next to next maximum multiplicity term with indices:

$$k_{1'}=m_{1'}=\omega_{1'}\neq k_{2'}=m_{2'}=\omega_{2'}\neq\cdots\neq k_{(n-s)'}=m_{(n-s)'}=\omega_{1'}\ \text{... third max multiplicity.} \tag{139}$$

Note that here we are considering only a particular permutation term of the third maximum multiplicity. The corresponding term is given by

$$a^4_{\omega_{1'}} a^2_{\omega_{2'}} \cdots a^2_{\omega_{(n-2)'}} \lambda \times \left(\alpha'^{(i_{1'})}_{\omega_{1'}} \alpha'^{(\omega_{1'})}_{j_{1'}} \cdots \alpha'^{(i_{(n-2)'})}_{\omega_{(n-2)'}} \alpha'^{(\omega_{(n-2)'})}_{j_{(n-2)'}} \alpha'^{(i_{(n-1)'})}_{\omega_{1'}} \alpha'^{(\omega_{1'})}_{j_{(n-1)'}} p'_{\omega_{1'} j_{1'}} \cdots p'_{\omega_{(n-1)'} j_{(n-1)'}} \varepsilon_{i_1 \cdots i_n} \varepsilon_{j_1 \cdots j_n} \right). \tag{140}$$

Now if we replace $i_{1'}$ by $i_{(n-1)'}$ then the expression devoid of the Levi-Civita tensor remains the same but with a different sign and hence they cancel each other. This means the contribution of this third maximum multiplicity term is zero. We can extend the statement to include the third maximum multiplicity terms of different permutation and infer that they all cancel each other rendering a vanishing contribution to the $s = 1$ term.

Also owing to the similarity in the endoskeletal structure of the lower multiplicity terms, the argument can be easily extended to these terms and we can conclude that all of them do not have any contribution. This means only the maximum and next to maximum multiplicity terms have a contribution to the $s = 1$ term and hence if any two of the $a'_i s$ are zero, the $s = 1$ term will vanish. And hence Eq. (122) will become of the form:

$$\sum_{s=2}^{n} \lambda^s a_{k_{1'}} a_{m_{1'}} \cdots a_{k_{(n-s)'}} a_{m_{(n-s)'}} \times \left(\alpha'^{(i_{1'})}_{k_{1'}} \alpha'^{(m_{1'})}_{j_{1'}} \cdots \alpha'^{(i_{(n-s)'})}_{k_{(n-s)'}} \alpha'^{(m_{(n-s)'})}_{j_{(n-s)'}} p'_{k_{1'} j_{1'}} \cdots p'_{k_{(n-s)'} j_{(n-s)'}} \varepsilon_{i_1 \cdots i_n} \varepsilon_{j_1 \cdots j_n} \right) = 0. \tag{141}$$

Here we can take out λ^2 common and consequently two of the solutions will be trivial. This proves Eq. (59). Once again the second line terms in Eq. (52) give rise to hyperboloid with two flat axes and hence the final result remains the same. Now for the cases of $s \geq 2$, we can extend the arguments of the proof and conclude that s of the solutions will be trivial.

General s

The arguments above can be easily extended to include the case of general s. All the higher multiplicity terms up to sth maximum multiplicity follow the arguments of proofs presented above. Since we don't have a common ω whenever we replace $i'_{k'} s$, we have to replace $\omega'_{k'} s$ and followed by $j'_{k'} s$ in order to get a similar form but with the same sign. And the moment we get the $(s+1)$th maximum multiplicity term, we have a common ω, and the replacement of the $i'_{k'} s$ does not matter anymore, which leads to the cancellation of these kinds of terms. So the coefficient of the λ^s term in Eq. (122) contains terms with at least sth maximum multiplicity and higher ones. And hence they have s trivial solutions.

External mathematica codes

Here we give the details of the mathematica codes we have provided in order to reproduce Fig. 13. So given the external momenta and the masses of all the loop and internal propagators, we can reproduce the final figure. First of all, we reproduce the triangles of Figs. 6 and 7 corresponding to the triangle, bubble, and tadpole Feynman diagrams in Triangle.nb, Bubble.nb, and Tadpole.nb, respectively. Then we add up all the contributions in Finalfig.nb. Finally, we give the corresponding quadric surface diagrams in the notebooks.

Triangle.nb

This is the first notebook to be read in the series of the notebooks. Here we have described that, given the credentials of the external momenta p_{ij} and the loop propagator masses m_i, how to find the center 'c' of the original sphere in Eq. (100) inside the triangle corresponding to the triangle Feynman diagram. In order to do that, we use the property that the center 'c' is equidistant from the tip of the mass vectors in Fig. 16. Then we set $c = 0$ following our convention of keeping the center at the origin. Using this, we find out the coordinates of the vertices of our triangles with reference to the origin as the center of the sphere. In this way, we get the triangle corresponding to the triangle Feynman diagram.

Bubble.nb

For the bubble Feynman diagrams, we use the property that two of the vertices of the triangle corresponding to them coincide with the triangle corresponding to the triangle Feynman diagram. The third vertex is given by

$p_{ij} - r_B$ if the first two vertices are given by p_i and p_j. The shift r_B is decided by the masses of the internal propagators from the bubble Feynman diagrams, see Eq. (107). Finally, we take the mirror image of the third vertex about the line joining the first two vertices so that the triangle corresponding to the bubble Feynman diagram falls outside the original triangle when all the triangles are stacked up in the final figure, see Finalfig.nb.

Tadpole.nb

After the triangles corresponding to the bubble and the triangle Feynman diagrams are created (Triangle.nb, Bubble.nb), we can construct the triangles corresponding to the tadpole Feynman diagrams. One of the vertex p_i is the same as the original triangle and the bubble, as evident in Table 1, one more vertex is the same as the bubble $p_{ij} - r_B$ and the third vertex vector is proportional to the first vertex vector with magnitude depending upon the internal propagator mass. We have denoted it here by F1. Finally, we take the reflection of the second and the third about the line p_{ij} so that the tadpole triangle falls outside the original triangle when all the triangles are stacked up in the final figure, see Finalfig.nb.

Finalfig.nb

Finally, we stack up all the triangles in order to get the final figure in Fig. 13. Note that we are not reproducing Fig. 15 where the denominator consideration is taken care of.

References

1. J.L. Bourjaily, E. Gardi, A.J. McLeod et al., All-mass n-gon integrals in n dimensions. J. High Energ. Phys. **2020**, 29 (2020). https://doi.org/10.1007/JHEP08(2020)029
2. Lionel Mason and David Skinner, J. Phys. A: Math. Theor. **44**, 135401 (2011)
3. G. Dian, P. Heslop, Amplituhedron-like geometries. J. High Energ. Phys. **2021**, 74 (2021). https://doi.org/10.1007/JHEP11(2021)074
4. N. Arkani-Hamed, J. Bourjaily, F. Cachazo et al., A note on polytopes for scattering amplitudes. J. High Energ. Phys. **2012**, 81 (2012). https://doi.org/10.1007/JHEP04(2012)081
5. M.F. Paulos, M. Spradlin, A. Volovich, Mellin amplitudes for dual conformal integrals. J. High Energ. Phys. **2012**, 72 (2012). https://doi.org/10.1007/JHEP08(2012)072
6. A. Hodges, Eliminating spurious poles from gauge-theoretic amplitudes. J. High Energ. Phys. **2013**, 135 (2013). https://doi.org/10.1007/JHEP05(2013)135
7. D. Nandan, M.F. Paulos, M. Spradlin et al., Star integrals, convolutions and simplices. J. High Energ. Phys. **2013**, 105 (2013). https://doi.org/10.1007/JHEP05(2013)105
8. M.F. Paulos, Loops, polytopes and splines. J. High Energ. Phys. **2013**, 7 (2013). https://doi.org/10.1007/JHEP06(2013)007
9. B. Ananthanarayan, A.B. Das, R. Sarkar, Asymptotic analysis of Feynman diagrams and their maximal cuts. Eur. Phys. J. C **80**, 1131 (2020). https://doi.org/10.1140/epjc/s10052-020-08609-0
10. B. Ananthanarayan, A.B. Das, D. Wyler, Hopf algebra structure of the two loop three mass nonplanar Feynman diagram. Phys. Rev. D (2021). https://doi.org/10.1103/PhysRevD.104.076002
11. S. Abreu, R. Britto, C. Duhr et al., Cuts from residues: the one-loop case. J. High Energ. Phys. **2017**, 114 (2017). https://doi.org/10.1007/JHEP06(2017)114
12. H. Elvang, Y. Huang, *Scattering Amplitudes in Gauge Theory and Gravity* (Cambridge University Press, Cambridge, 2015). https://doi.org/10.1017/CBO9781107706620
13. J.M. Henn, J.C. Plefka, Scattering amplitudes in gauge theories. Lect. Notes Phys. **883**, 1 (2014)
14. N. Arkani-Hamed, J. Trnka, The Amplituhedron. J. High Energ. Phys. **2014**, 30 (2014). https://doi.org/10.1007/JHEP10(2014)030
15. N. Arkani-Hamed, Y. Bai, S. He et al., Scattering forms and the positive geometry of kinematics, color and the worldsheet. J. High Energ. Phys. **2018**, 96 (2018). https://doi.org/10.1007/JHEP05(2018)096
16. N. Arkani-Hamed, J. Bourjaily, F. Cachazo, A. Goncharov, A. Postnikov, J. Trnka, *Grassmannian Geometry of Scattering Amplitudes* (Cambridge University Press, Cambridge, 2016). https://doi.org/10.1017/CBO9781316091548
17. L., Ferro, Ł., Tomasz, Amplituhedra, and beyond. J. Phys. A: Math. Theor. **54**, n. pag (2020)
18. N. Arkani-Hamed, S. He, G. Salvatori et al., Causal diamonds, cluster polytopes and scattering amplitudes. J. High Energ. Phys. **2022**, 49 (2022). https://doi.org/10.1007/JHEP11(2022)049
19. G. Salvatori, S.L. Cacciatori, Hyperbolic geometry and amplituhedra in 1+2 dimensions. J. High Energ. Phys. **2018**, 167 (2018). https://doi.org/10.1007/JHEP08(2018)167
20. G. Salvatori, 1-loop amplitudes from the Halohedron. J. High Energ. Phys. **2019**, 74 (2019). https://doi.org/10.1007/JHEP12(2019)074

21. P. Banerjee, A. Laddha, P. Raman, Stokes polytopes: the positive geometry for ϕ^4 interactions. J. High Energ. Phys. **2019**, 67 (2019). https://doi.org/10.1007/JHEP08(2019)067
22. P.B. Aneesh, M. Jagadale, N. Kalyanapuram, Accordiohedra as positive geometries for generic scalar field theories. Phys. Rev. D (2019). https://doi.org/10.1103/PhysRevD.100.106013
23. O. Schnetz, The geometry of one-loop amplitudes. 2010. arXiv e-prints. arXiv:1010.5334S (2010)
24. A.I. Davydychev, R. Delbourgo, A geometrical angle on Feynman integrals. J. Math. Phys. **39**, 4299–4334 (1998). https://doi.org/10.1063/1.532513
25. C. Duhr, A. Klemm, F. Loebbert, C. Nega, F. Porkert, Yangian-invariant fishnet integrals in two dimensions as volumes of Calabi-Yau varieties. Phys. Rev. Lett. (2023). https://doi.org/10.1103/PhysRevLett.130.041602
26. N. Arkani-Hamed, T. Lam, M. Spradlin, Non-perturbative geometries for planar $\mathcal{N} = 4$ SYM amplitudes. J. High Energ. Phys. **2021**, 65 (2021). https://doi.org/10.1007/JHEP03(2021)065
27. B. Ananthanarayan, S. Bera, T. Pathak, Nucl. Phys. B **995**, 116345 (2023). https://doi.org/10.1016/j.nuclphysb.2023.116345
28. A.I. Davydychev, J. Math. Phys. **32**, 1052 (1991). https://doi.org/10.1063/1.529383
29. https://renormalizationgroupllc.net/tag/levi-civita/
30. N. Johnston, *Advanced Linear and Matrix Algebra* (Springer, Switzerland, 2021)
31. K. Riley, M. Hobson, S. Bence, *Mathematical Methods for Physics and Engineering: A Comprehensive Guide*, 3rd edn. (Cambridge University Press, Cambridge, 2006). https://doi.org/10.1017/CBO9780511810763